Supporting Information for the Paper Entitled:

"A Well-Defined Isocyano Analogue of $HCo(CO)_4$. Synthesis, Decomposition and Catalytic 1,1-Hydrogenation of Isocyanides."

Alex E. Carpenter, Arnold L. Rheingold and Joshua S. Figueroa*

Department of Chemistry and Biochemistry, University of California, San Diego, 9500 Gilman Drive, Mail Code 0358, La Jolla, California 92093-0258

Email: jsfig@ucsd.edu

Contents:

S1. Synthetic Procedures and Characterization Data.

S1.1. General Considerations. Unless otherwise stated, all manipulations were carried out under an atmosphere of dry dinitrogen using standard Schlenk and glovebox techniques. Solvents were dried and deoxygenated according to standard procedures.[1,2,3] Reagent grade starting materials were purchased from commercial sources and were used as received or purified by standard procedures.[1,2] The compounds $CNAr^{Mes2}$, $^{13}CNAr^{Mes2}$, and $Na[Co(CNAr^{Mes2})_4]$ were prepared according to literature procedures.[3,4,5] Benzene-d_6, and THF-d_8 (Cambridge Isotope Laboratories) were dried over NaK/benzophenone, vacuum distilled, degassed and stored over a mixture of 3 and 4 Å molecular sieves for 2 d prior to use. Solution ^1H, ^2H, $^{13}C\{^1H\}$ and $^{31}P\{^1H\}$ were recorded on Varian Mercury 300 and 400 MHz spectrometers, a Varian X-Sens 500 MHz spectrometer, or a JEOL ECA 500 MHz spectrometer. ^1H and $^{13}C\{^1H\}$ NMR chemical shifts are reported in ppm relative to $SiMe_4$ (^1H and $^{13}C\{^1H\}$ δ = 0.0 ppm) with reference to residual protio resonances of 7.16 ppm (^1H) and 128.06 ppm (^{13}C) for benzene-d_6, 3.58 ppm (^1H) and 67.21 (^{13}C) for THF-d_8. $^{31}P\{^1H\}$ NMR chemical shifts are reported in ppm relative to an internal standard of 85% H_3PO_4 (0 ppm) in a sealed capillary. FTIR spectra were recorded on a Thermo-Nicolet iS10 FTIR spectrometer. Samples were prepared either as KBr pellets or as C_6D_6 solutions injected into a ThermoFisher solution cell equipped with KBr windows. For solution FTIR spectra, solvent peaks were digitally subtracted from all spectra by comparison with an authentic spectrum obtained immediately prior to that of the sample. The following abbreviations are used for the intensities and characteristics of important IR absorption bands: vs = very strong, s = strong, m = medium, w = weak, vw = very weak, b = broad, vb = very broad, sh = shoulder. Combustion analyses were performed by Robertson Microlit Laboratories of Ledgewood, NJ (USA). High-resolution mass spectra were recorded on an Agilent 6230 Accurate-Mass TOFMS running in positive ion mode.

S1.2. Synthesis of $HCo(CNAr^{Mes2})_4$ (1): An Et_2O solution of $Na[Co(CNAr^{Mes2})_4$ (1.500 g, 1.04 mmol, 200 mL) was cooled to –100 ˚C and solid 3,5-dimethylbenzoic acid (0.159 g, 1.09 mmol, 1.05 equiv) was added. The reaction mixture allowed to warm from –100 ˚C to –35 ˚C, where it was stirred for 1 h. During this time, the reaction mixture turned from a homogenous, brick-red solution to a dark, orange slurry. The reaction mixture was then concentrated to a solid under reduced pressure. The solid was dissolved in C_6H_6 (50 mL) and filtered twice using medium porosity fritted funnels packed with Celite. The C_6H_6 was then lyophilized from the resulting filtrate to afford a fine yellow-orange powder. This material was suspended in MeCN (20 mL) and filtered. The yellow filter cake was washed with MeCN (3 x 30 mL), Et_2O (3 x 5 mL) and *n*-pentane (3 x 2 mL). This precipitate cake was collected and dried *in vacuo* to afford a bright, yellow-orange powder. Yield: 1.19 g, 0.839 mmol, 80.7%. Single crystals of $HCo(CNAr^{Mes2})_4$ may be obtained from a concentrated MeCN/Toluene (70:30 v/v); Cyclohexane/THF (70:30 v/v), or *n*-pentane/THF (70:30 v/v) solutions stored at –35 ˚C. ^1H NMR (400.1 MHz, C_6D_6, 20 ˚C): δ = 6.90 (t, 4H, *p*-Ph), 6.98 (d, 8H, *m*-Ph), 6.86 (s, 16H, *m*-Mes), 2.27 (s, 24H *p*-Mes), 2.01 (s, 48H, *o*-Mes), –13.10 (s, 1H, Co–*H*) ppm. ^1H NMR (300.1 MHz, THF-d_8, 20 ˚C): δ = 7.19 (t, 4H, *p*-Ph, 7.2 Hz), 6.96 (d, 8H, *m*-Ph, 7.2 Hz), 6.73 (s, 16H, *m*-Mes), 2.17 (s, 24H, *p*-Mes), 1.81 (s, 48H, *o*-Mes), –13.37 (s, 1H, Co–*H*) ppm.

$^{13}C\{^{1}H\}$ NMR (125.8 MHz, C_6D_6, 20 ˚C): δ = 182.9 (*C*NR), 138.1, 136.8, 136.5, 136.4, 132.0, 131.2, 129.4, 125.3, 21.8 (*p*-Mes), 21.3 (*o*-Mes) ppm. FTIR (C_6D_6; KBr Window, 25 ˚C): ν_{CN} = 2076 (w), 2013 (s), 1957 (vs) cm^{-1} also, 2998 (vw, sh), 2956 (vw), 2917 (w), 2856 (w), 1612 (w), 1578 (m), 1489 (w), 1459 (w), 1441 (w), 1410 (m), 1377 (w), 1271 (vw), 1199 (vw), 1032 (w), 852 (m), 777 (vw), 755 (w), 757 (w), 739 (vw), 603 (vw), 566 (vw) cm^{-1}. FTIR (KBr Pellet, 25 ˚C): ν_{CN} = 2090 (w), 2018 (s), 1963 (vs) cm^{-1} also, 2949 (w), 2918 (m), 2858 (w), 1613 (m), 1579 (m), 1488 (w), 1453 (m), 1405 (m), 1376 (m), 1273 (vw), 1242 (vw), 1198 (w), 1032 (m), 850 (m), 802 (m), 778 (w), 755 (s), 741 (vw), 651 (vw), 603 (vw), 563 (vw), 517 (w) cm^{-1} (ν_{CoH} was not unambiguously located, presumably due to overlap with intense ν_{CN} stretches). Anal. Calcd. For $C_{100}H_{101}N_4Co$: C, 84.71; H, 7.18; N, 3.95. Found: C, 83.97; H, 7.17; N, 3.84.

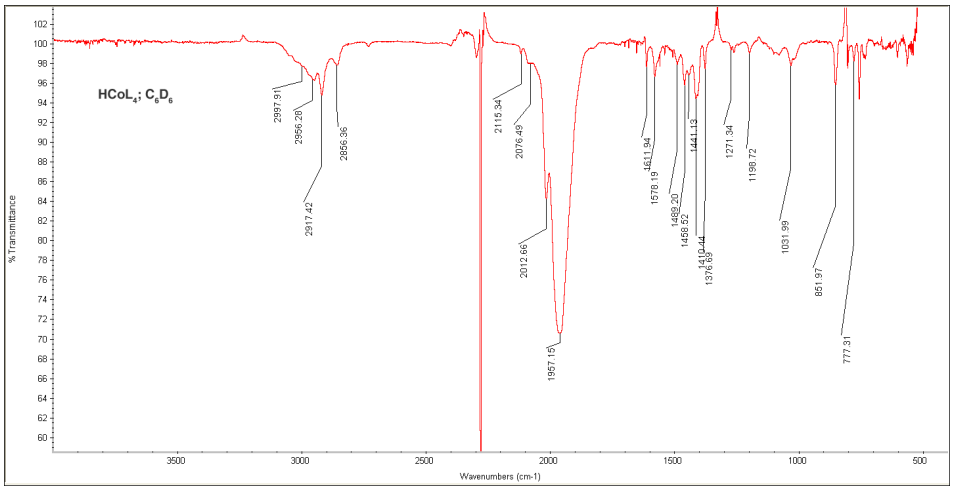

Figure S1.1. Baseline-corrected, solution-state IR Spectrum (C_6D_6) of $HCo(CNAr^{Mes2})_4$ (**1**). Solvent background (C_6D_6) for subtraction was obtained immediately prior to experiment.

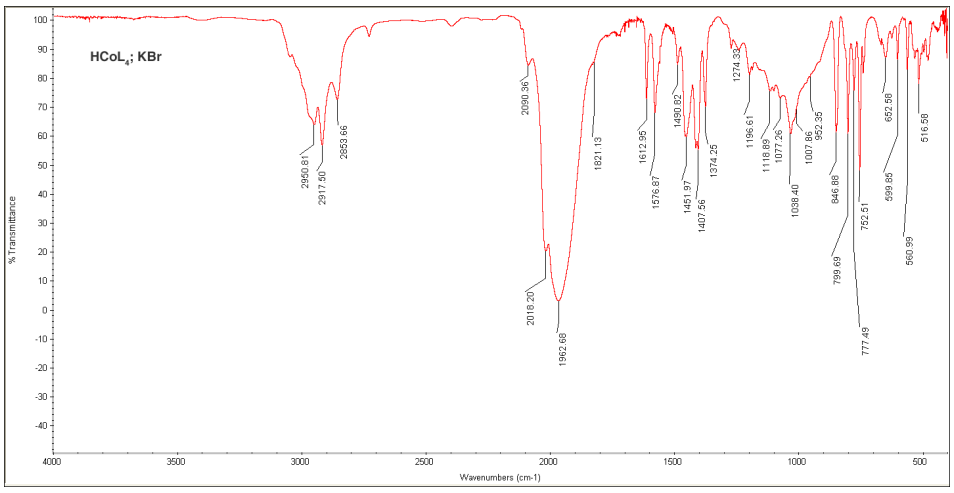

Figure S1.2. Baseline-corrected, solid-state IR Spectrum (KBr Pellet) from crystalline sample of $HCo(CNAr^{Mes2})_4$ (**1**).

S1.3. Synthesis of HCo(^{13}CNAr^{Mes2})$_4$: This material was prepared by the same methodology reported for HCo(CNAr^{Mes2})$_4$, but on reduced scale: Na[Co(^{13}CNAr^{Mes2})$_4$ (0.120 g, 0.083 mmol); 3,5-dimethyl benzoic acid (0.012 g, 0.086 mmol, 1.03 equiv). Yield: 0.066 g, 0.046 mmol, 56.0 %. FTIR (C_6D_6; KBr Window, 25 ˚C): ν_{CN} = 2085 (w), 2002 (s), 1924 (vs) cm^{-1} also, 2956 (w), 2915 (m), 2851 (w), 1580 (m), 1563 (m), 1416 (m), 1277 (m), 1249 (m), 1186 (m), 1047 (m), 853 (m), 775 (w), 755 (w) cm^{-1}.

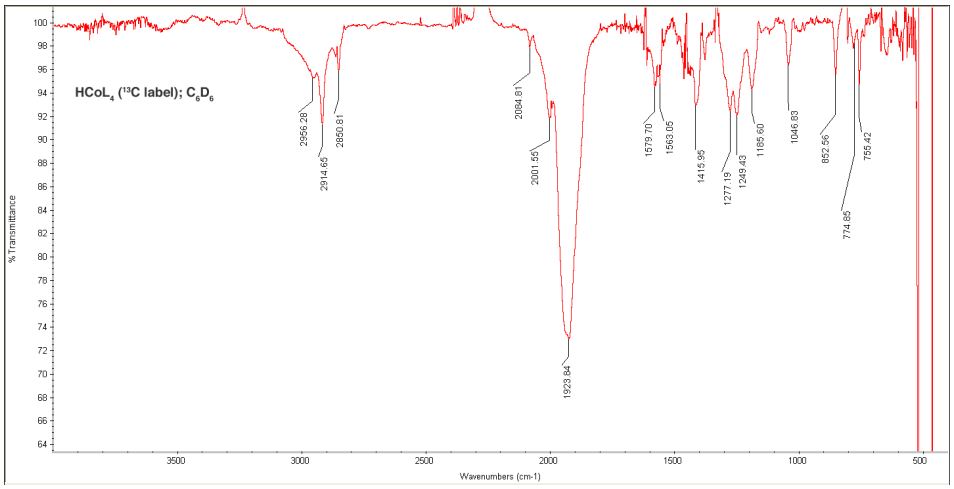

Figure S1.3. Baseline-corrected, solution-state IR Spectrum (C_6D_6) of HCo(^{13}CNAr^{Mes2})$_4$ (**1**-^{13}C). Solvent background (C_6D_6) for subtraction was obtained immediately prior to experiment.

S1.4. Synthesis of DCo(CNAr^{Mes2})$_4$ (1-*d*$_1$): Step 1: Preparation of deuterated 3,5-dimethylbenzoic acid. To a stirring Et_2O solution of 3,5-dimethylbenzoic acid (1.00 g, 6.66 mmol, 30 mL), sodium hydride (0.32 g, 13.3 mmol, 2 equiv) was added as a gray powder. Effervescence and concomitant formation of a colorless precipitate occurred rapidly. To this reaction mixture, a 35% by weight DCl in D_2O solution (2.7 mL, 33.3 mmol, 5 equiv) was added via syringe. The resulting solution was stirred for 1 h, concentrated to a colorless solid, under reduced pressure, and dried *in vacuo* for 18 h. The resulting material was dissolved in C_6H_6 (50 mL) and filtered through a medium porosity fritted funnel packed with Celite. The filtrate was concentrated to afford a colorless solid under reduced pressure. Yield: 0.9 g, 5.99 mmol, 89.9 %. ^{1}H NMR (500.2 MHz, C_6D_6, 20 ˚C): δ = 7.89 (s, 2H, *o*-Ph), 6.80 (s, 1H, *p*-Ph), 1.99 (s, 6H, C*H*$_3$). ^{2}H (76.8 MHz, C_6D_6, 20 ˚C): δ = 12.84 (s, 1D, O*D*). ^{13}C{^{1}H} NMR (125.8 MHz, C_6D_6, 20 ˚C): δ = 173.1 (*C*=O), 138.3 (*m*-Ph), 135.7 (*p*-Ph), 129.7 (*i*-Ph), 128.5 (*o*-Ph), 20.9 (*C*H$_3$). FTIR (C_6D_6, KBr windows, 25 ˚C): ν_{OD} = 2954 (vbr) cm^{-1}, ν_{CO} = 1728 (m) cm^{-1}, also 2954 (vs), 2920 (m), 2862 (w), 1609 (s), 1452 (m), 1422 (w), 1385 (m), 1360 (s), 1332 (w), 1309 (m), 1261 (m), 1241 (m), 1048 (w), 870 (w), 783 (w) cm^{-1}.

Step 2: **Preparation of DCo(CNAr^{Mes2})$_4$ (1-*d*$_1$):** This material was prepared by the same methodology reported for HCo(CNAr^{Mes2})$_4$, but on reduced scale. Na[Co(CNAr^{Mes2})$_4$ (0.300 g, 0.208 mmol); deuterated 3,5-dimethylbenzoic acid-*d*$_1$ (0.032 g, 0.219 mmol, 1.05 equiv). Yield: 0.143 g, 0.101 mmol, 48.6 %. ^{2}H NMR (76.8 MHz, 90:10 (C_6H_6/C_6D_6), 20 ˚C): δ = –13.1 (s, Co-*D*). FTIR (C_6D_6; KBr Window, 25 ˚C): ν_{CN} = 2079 (w), 2018 (s), 1963 (vs) cm^{-1} also, 2951 (vw), 2917 (w), 2859 (w), 1613 (w), 1577 (m),

1488 (w), 1455 (w), 1410 (m), 1377 (w), 1271 (vw), 1197 (vw), 1030 (w), 853 (m), 777 (vw), 755 (w) 736 (vw), 603 (vw), 564 (vw) cm^{-1}. FTIR (KBr Pellet, 25 ˚C): ν_{CN} = 2088 (w), 2015 (s), 1970 (vs) cm^{-1} also, 2953 (w), 2919 (m), 2857 (w), 1613 (m), 1577 (m), 1487 (w), 1457 (m), 1405 (m), 1376 (m), 1198 (w), 1032 (m), 850 (m), 802 (m), 778 (w), 755 (s), 741 (vw), 630 (vw), 604 (vw), 565 (vw), 517 (w) cm^{-1}.

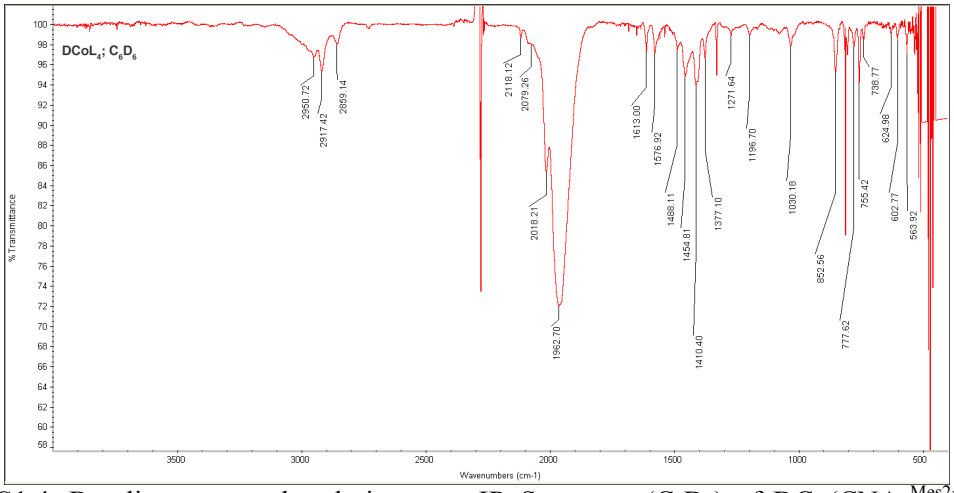

Figure S1.4. Baseline-corrected, solution-state IR Spectrum (C_6D_6) of $DCo(CNAr^{Mes2})_4$ (**1**-d_1). Solvent background (C_6D_6) for subtraction was obtained immediately prior to experiment.

S1.5. Synthesis and Isolation of Co(η^6-(Mes)-κ^1-*C*-C(H)NAr^{Mes2})(CNAr^{Mes2}) (2) via Decomposition of HCo(CNAr^{Mes2})$_4$ (1): A C_6H_6 solution of $HCo(CNAr^{Mes2})_4$ (0.200 g, 0.141 mmol, 5 mL) was stirred at room temperature for 15 h. During this time the reaction mixture turned from orange to a dark red solution. The reaction mixture was concentrated to a solid under reduced pressure. The resulting residue contained a 1:2 mixture of **2** and free $CNAr^{Mes2}$ as assessed by ^1H NMR spectroscopy. The two components displayed similar solubility properties in common organic solvents and could not be separated by fractional crystallization. Therefore, $CNAr^{Mes2}$ was separated by chemical conversion of Co(η^6-(Mes)-κ^1-*C*-C(H)NAr^{Mes2})(CNAr^{Mes2}) **(2)** to an insoluble aminocarbene salt. Pure Co(η^6-(Mes)-κ^1-*C*-C(H)NAr^{Mes2})(CNAr^{Mes2}) **(2)** was then isolated by washing and subsequent deprotonation (Figure S1.5.). These additional steps leading to pure Co(η^6-(Mes)-κ^1-*C*-C(H)NAr^{Mes2})(CNAr^{Mes2}) **(2)** are outlined below.

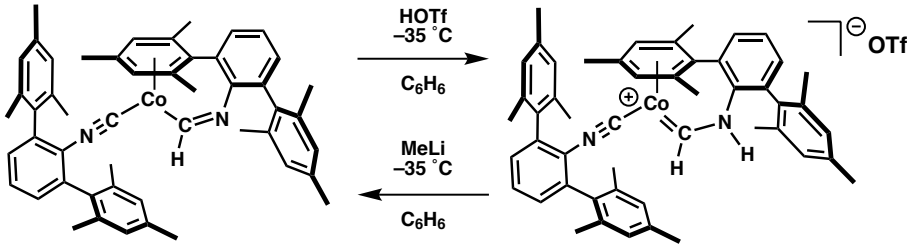

Figure S1.5. Reversible *N*-protonation of Co(η^6-(Mes)-κ^1-*C*-C(H)NAr^{Mes2})(CNAr^{Mes2}) (**2**) to afford an insoluble aminocarbene salt which can be separated from $CNAr^{Mes2}$.

Step 1: Synthesis of [Co(η^6-(Mes)-κ^1-*C*-C(H)N(H)Ar^{Mes2})(CNAr^{Mes2})]OTf via protonation Co(η^6-(Mes)-κ^1-*C*-C(H)NAr^{Mes2})(CNAr^{Mes2}) (2). To a C_6H_6 solution of the 1:2 mixture of Co(η^6-(Mes)-κ^1-*C*-C(H)NAr^{Mes2})(CNAr^{Mes2}) (**2**) and free CNAr^{Mes2} prepared above, was added triflic acid (HOTf; OTf = $[O_3SCF_3]^-$; 0.022 g, 0.148 mmol, 1.05 equiv). The reaction mixture was allowed to stir for 30 min resulting in the formation of an an orange precipitate. The mixture was then filtered through a medium porosity fritted funnel to afford an orange solid, which was washed with C_6H_6 (3 x 0.5 mL), *n*-pentane (3 x 5 mL) and Et_2O (3 x 1 mL). Yield: 0.080 g 0.090 mmol, 64.1%. Single crystals amenable for structural characterization (Figure S3.12) were obtained from a layering a THF solution with *n*-pentane, followed by storage at –35 ˚C.

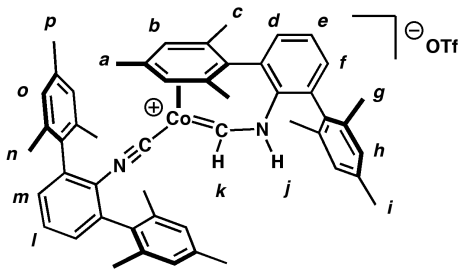

Figure S1.6. Labeling scheme for ^{1}H NMR assignments of [Co(η^6-(Mes)-κ^1-*C*-C(H)N(H)Ar^{Mes2})(CNAr^{Mes2})]OTf.

Data for [Co(η^6-(Mes)-κ^1-*C*-C(H)N(H)Ar^{Mes2})(CNAr^{Mes2})]OTf. ^{1}H NMR (499.8 MHz, THF-d_8, 20 ˚C): δ = 9.75 (d, 1H, *J* = 9 Hz, H_j), 8.54 (d, 1H, *J* = 9 Hz, H_k), 7.62 (dd, 1H, *J* = 7 Hz; *J* = 2 Hz, H_d), 7.58 (t, 1H, *J* = 7 Hz, H_l), 7.55 (t, 1H, *J* = 7 Hz, H_e), 7.23 (d, 2H, *J* = 8 Hz, H_m), 7.22 (dd, 1H, *J* = 7 Hz; *J* = 2 Hz, H_f), 7.09 (s, 2H, H_h), 6.95 (s, 4H, H_o), 6.33 (s, 2H, H_b), 2.36 (s, 3H, H_i), 2.15 (s, 6H, H_p), 2.02 (s, 6H, H_g), 1.97 (s, 6H, H_c), 1.43 (s, 3H, H_a) ppm. ^{13}C{^{1}H} NMR (100.6 MHz, THF-d_8, 20 ˚C): δ = 221.1 (*C*(H)N(H)R), 158.8 (*C*NR), 139.7, 139.5, 138.6, 137.8, 137.3, 136.6, 135.0, 133.5, 132.9, 132.3, 130.5, 130.3, 130.0, 129.8, 129.0, 128.8, 127.7, 121.6, 107.7, 107.2, 104.8, 96.4, 21.0, 20.8, 20.3, 20.2, 20.1, 19.5 ppm. FTIR (KBr Pellet, 25 ˚C): ν_{CN} = 2121 (vs) cm^{-1}, ν_{NH} = 3303 (s) cm^{-1} also, 3079 (vw), 3037 (vw), 2962 (w), 2918 (m), 2854 (w), 1610 (m), 1496 (m), 1460 (m), 1371 (s), 1313 (m), 1274 (s), 1224 (m), 1143 (s), 1082 (vb), 1030 (s), 861 (w), 808 (m), 760 (m), 633 (m), 569 (w), 539 (w), 511 (w) cm^{-1}. Anal. Calcd. For $C_{51}H_{52}N_2CoF_3O_3S$: C, 68.91; H, 5.90; N, 3.15. Found: C, 66.78; H, 5.01; N, 3.03. Multiple attempts to acquire satisfactory elemental analysis were unsuccessful. We tentatively attribute this observation to the presence of Co-containing insoluble impurities.

Step 2: Isolation of of Co(η^6-(Mes)-κ^1-*C*-C(H)NAr^{Mes2})(CNAr^{Mes2}) (2) via Deprotonation of [Co(η^6-(Mes)-κ^1-*C*-C(H)N(H)Ar^{Mes2})(CNAr^{Mes2})]OTf. [Co(η^6-(Mes)-κ^1-*C*-C(H)N(H)Ar^{Mes2})(CNAr^{Mes2})]OTf (0.120 g, 0.135 mmol) was dissolved in THF (5 mL) and cooled to –35 ˚C. To this solution was added solid MeLi (0.003 g, 0.139 mmol, 1.03 equiv) and the reaction mixture was allowed to stir while warming to room temperature for 1 h. All volatiles were then removed under reduced pressure. The resulting solid was extracted with C_6H_6

(2 mL) and filtered twice through medium porosity fritted funnels packed with Celite to remove LiOTf. The filtrate was dried, under vacuum, to a red solid. Yield: 0.095 g, 0.129 mmol, 95.6%. Single crystals of **2** were from storage of 70:30 *n*-pentane/C_6H_6 mixture at –35 ˚C for 2 d.

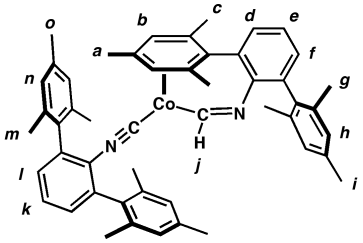

Figure S1.7. Labeling scheme for ^{1}H NMR assignments of Co(η^6-(Mes)-κ^1-*C*-C(H)NAr^{Mes2})(CNAr^{Mes2}) (**2**).

Data for Co(η^6-(Mes)-κ^1-*C*-C(H)NAr^{Mes2})(CNAr^{Mes2}) (2): ^{1}H NMR (400.1 MHz, C_6D_6, 20 ˚C): δ = 8.73 (s, 1H, H_j), 7.25 (dd, 1H, J = 7 Hz; J = 2 Hz, H_d), 7.21 (dd, 1H, J = 7 Hz; J = 2 Hz, H_f), 7.15 (t, 1H, J = 7 Hz, H_e), 7.04 (s, 2H, H_h), 6.92 (t, 1H, J = 7 Hz, H_k), 6.83 (d, 2H, J = 7 Hz, H_l), 6.79 (s, 4H, H_n), 5.36 (s, 2H, H_b), 2.36 (s, 3H, H_i), 2.27 (s, 6H, H_o), 2.09 (s, 6H, H_g), 2.05 (s, 12H, H_m), 1.75 (s, 6H, H_c), 1.20 (s, 3H, H_a) ppm. ^{13}C{^{1}H} NMR (125.8 MHz, C_6D_6, 20 ˚C): δ = 205.0 (*C*(H)NR), 170.1 (*C*NR; br), 150.5, 140.8, 139.8, 137.9, 137.7, 136.0, 135.9, 135.5, 135.3, 130.6, 129.5, 129.3, 128.8, 127.5, 126.7, 125.9, 124.1, 118.7, 100.3, 100.2, 100.0, 99.7, 21.4, 21.3, 21.0, 20.5, 20.3, 19.5 ppm. FTIR (C_6D_6, KBr windows, 25 ˚C): ν_{CN} = 2057 (vs), 2015 (s) (two bands due to coupling with other vibronic modes) cm^{-1}, $\nu_{(H)C=NR}$ = 1485 (s) cm^{-1} also, 3048 (vw), 3026 (vw), 2979 (w), 2942 (w), 1613 (m), 1513 (m), 1455 (m), 1407 (m), 1377 (w), 1299 (m), 1119 (m), 1069 (s), 1039 (s), 852 (m), 755 (m), 688 (w), 631 (w), 564 (w) cm^{-1}. FTIR (KBr Pellet, 25 ˚C): ν_{CN} = 2054 (vs), 2013 (s) (two bands due to coupling with other vibronic modes) cm^{-1}, $\nu_{(H)C=NR}$ = 1482 (s) cm^{-1} also, 3026 (vw), 2965 (w), 2915 (w), 2853 (w), 1609 (w), 1569 (vw), 1512 (m), 1459 (m), 1411 (m), 1377 (w), 1308 (m), 1272 (m), 1181 (m), 1045 (m), 1031 (m), 848 (m), 815 (m), 802 (m), 793 (m), 754 (m), 737 (w), 690 (m), 677 (w), 649 (w), 632 (w), 543 (w) 520 (vw), 406 (w) cm^{-1}. Anal. Calcd. For $C_{50}H_{51}N_2Co$: C, 81.28; H, 6.96; N, 3.79. Found: C, 80.52; H, 7.08; N, 3.44.

Supplemental Characterization Data For Co(η^6-(Mes)-κ^1-*C*-^{13}C(H)NAr^{Mes2})(^{13}CNAr^{Mes2}): ^{13}C-labeled Co(η^6-(Mes)-κ^1-*C*-^{13}C(H)NAr^{Mes2})(^{13}CNAr^{Mes2}) was prepared by the same methodology reported for non-isotopically enriched samples using HCo(^{13}CNAr^{Mes2})$_4$. A proton-coupled ^{13}C NMR was acquired to confirm the presence of $^1J_{C\text{-}H}$ coupling between the iminoformyl carbon and proton.

S1.6. Synthesis of Co(η^6-(Mes)-κ^1-*C*-C[C(H)NAr^{Mes2}]NAr^{Mes2})(CNAr^{Mes2}) (3). Free CNAr^{Mes2} (0.069 g, 0.203 mmol, 1.0 equiv) was added to a stirring C_6H_6 solution of Co(η^6-(Mes)-κ^1-*C*-C(H)NAr^{Mes2})(CNAr^{Mes2}) (**2**; 0.150 g, 0.203 mmol, 5 mL). The reaction mixture was then heated in a sealed ampule to 60 ˚C for 3 d. Thereafter, it was concentrated to a solid under reduced pressure. The solid was dissolved in a minimal amount of C_6H_6, filtered and stored at 25 ˚C for 5 d to afford red single crystals that were collected and dried *in vacuo*. Yield: 0.032 g, 0.030 mmol. 14.6 %.

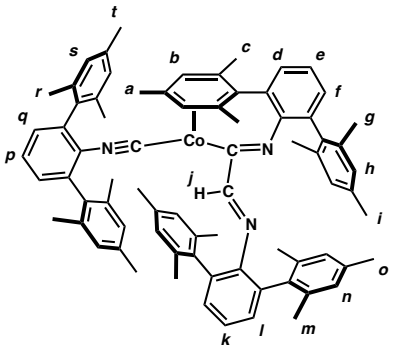

Figure S1.8. Labeling scheme for ^{1}H NMR assignments of Co(η^6-(Mes)-κ^1-*C*-C[C(H)NAr^{Mes2}]NAr^{Mes2})(^{13}CNAr^{Mes2}) (**3**).

Data for Co(η^6-(Mes)-κ^1-*C*-C[C(H)NAr^{Mes2}]NAr^{Mes2})(CNAr^{Mes2}) (3): ^{1}H and ^{13}C{^{1}H} NMR signals corresponding to the inserted C(H)NAr^{Mes2} moiety are significantly broadened, presumably due to hindered rotation of the diimine unit. ^{1}H NMR assignments are tentative. ^{1}H NMR (499.9 MHz, C_6D_6, 20 ˚C): δ = 7.34 (t, 1H, *J* = 7 Hz, H_p), 7.28 (dd, 1H, *J* = 7 Hz; *J* = 2 Hz, H_d), 7.14 (t, 1H, *J* = 7 Hz, H_e), 7.01 (d, 2H, *J* = 7Hz, H_q), 7.00 (br t, 1H, *J* = 7 Hz, H_k), 6.92 (dd, 1H, *J* = 7 Hz; *J* = 2 Hz, H_f), 6.76 (s, 1H, H_j), 6.74 (vbr, *J* = 7 Hz, H_l), 6.66 (vbr s, 4H, H_n), 6.56 (br s, 4H, H_s), 5.64 (br s, 1H, H_b), 4.49 (br s, 1H, H_b), 2.46 (s, 3H, H_i), 2.23 (s, 6H, H_g), 2.13 (s, 6H, H_t), 1.93–1.75 (vbr s, 24 H_m and H_r), 1.69 (s, 6H, H_o), 1.66 (br s, 6H, H_c), 0.41 (vb s, 3H, H_a) ppm. ^{13}C{^{1}H} NMR (125.8 MHz, C_6D_6, 20 ˚C): δ = 212.9 (RN*C*(C(H)NR), 204.9 (RNC(*C*(H)NR), 159.2 (*C*NR), 151.2, 150.2, 141.2, 140.7, 140.1, 138.2 (vbr), 137.4 (vbr), 137.2, 136.4 (vbr), 136.8 (br), 136.2, 135.9, 135.8, 135.1, 134.9, 133.2, 131.0, 130.2, 130.1, 129.7 (vbr), 129.3 (vbr), 129.1, 129.0, 128.8 (vbr), 128.4 (br), 127.9, 127.4, 124.0, 123.1, 120.1, 106.9 (vbr), 103.4, 103.2 (vbr), 101.3, 99.3 (vbr), 95.63 (vbr), 22.1 (vbr), 21.9 (vbr), 21.6 (br), 21.4 (vbr), 21.1, 21.0, 20.9, 20.0 ppm. HRMS (ESI; MeCN): m/z Calcd for $[C_{75}H_{77}N_3Co]^+$: 1078.5444; m/z Found: 1078.5440.

S1.7. Synthesis of HCo(CNAr^{Mes2})$_3$(CN*t*-Bu) (4$^{CNt\text{-}Bu}$): HCo(CNAr^{Mes2})$_4$ (**1**, 0.100 g, 0.071 mmol) was dissolved in THF (20 mL) and allowed to stir for 5 min. To this solution, CN*t*-Bu (0.007 g, 0.085 mmol, 1.2 equiv) was added via syringe. The resulting solution was allowed to stir at room temperature for 16 h. The solution was then concentrated to an orange solid under reduced pressure. This solid was suspended in MeCN (1 mL) and filtered. The resulting solid was washed with MeCN (3 x 5 mL) and *n*-pentane (4 x 0.25 mL) to afford a bright yellow powder. Yield: 0.038 g, 0.033 mmol 46.4%. ^{1}H NMR (400.1 MHz, C_6D_6, 20 ˚C): δ = 6.97-6.89 (m, 9H, *m*-Ph and *p*-Ph), 6.85 (s, 12H, *m*-Mes), 2.27 (s, 18H, *p*-Mes), 2.07 (s, 36H, *o*-Mes), 0.97 (s, 9H, *t*-Bu), –12.80 (s, 1H, Co–*H*) ppm. ^{13}C{^{1}H} NMR (100.6 MHz, C_6D_6, 20 ˚C): δ = 183.6 (*C*NR, CNAr^{Mes2}), 166.6 (*C*NR, CN*t*-Bu), 137.7, 136.5, 136.5, 136.1, 132.3, 129.6, 128.7, 125.1, 54.8 (N-*C*(CH$_3$)$_3$) , 30.4 (C(*C*H$_3$)$_3$), 21.5 (*p*-Mes), 20.6 (*o*-Mes) ppm. FTIR (C_6D_6, KBr windows, 25 ˚C): CN*t*-Bu ν_{CN} 2134 (m) cm^{-1}, CNAr^{Mes2} ν_{CN} = 2049 (s), 2029 (s), 1965 (vs) cm^{-1}, also 3048 (vw sh), 2980 (w), 2947 (w), 2918 (w), 2858 (vw), 1613 (m), 1578 (m), 1454 (m), 1413 (m), 1216 (w), 1032 (vw), 850 (m), 756 (m), 699 (bw) cm^{-1} (ν_{CoH}

was not unambiguously located, presumably due to overlap with intense ν_{CN} stretches). Anal. Calcd. For $C_{80}H_{84}N_4Co$: C, 82.80; H, 7.30; N, 4.83. Found: C, 82.47; H, 7.30; N, 4.73.

S1.8. Synthesis of $HCo(CNAr^{Mes2})_3(CNXyl)$ (4^{CNXyl}): $HCo(CNAr^{Mes2})_4$ (**1**, 0.100 g, 0.071 mmol) was dissolved in THF (50 mL) and allowed to stir for 5 min. To this reaction mixture, a THF solution of CNXyl (0.010 g, 0.078 mmol, 2 mL, 1.1 equiv) was added. The resulting solution was allowed to stir at room temperature for 16 h. Thereafter, the reaction mixture was concentrated to a dark orange solid under reduced pressure. It was then suspended in MeCN (1 mL) and filtered. The solid was washed with MeCN (2 x 0.5 mL) and *n*-pentane (4 x 0.25 mL) to afford a bright yellow powder. Yield: 0.045 g, 0.0319 mmol, 53%. ^{1}H NMR (500.2 MHz, C_6D_6, 20 ˚C): δ = 6.94 (t, 3H, J = 7 Hz, *p*-Ph $CNAr^{Mes2}$), 6.90 (d, 6H, J = 7 Hz, *m*-Ph $CNAr^{Mes2}$), 6.88 (d, 2H, J = 7 Hz, *m*-Ph CNXyl), 6.87 (t, 1H, J = 7 Hz, *p*-Ph CNXyl), 6.79 (s, 12H, *m*-Mes), 2.19 (s, 18H *p*-Mes), 2.05 (s, 36H, *o*-Mes $CNAr^{Mes2}$), 2.04 (s, 6H, CH_3 Xyl), –12.08 (s, 1H, Co–*H*) ppm. $^{13}C\{^1H\}$ NMR (125.8 MHz, C_6D_6, 20 ℃): δ = 184.0 (*C*NR, $CNAr^{Mes2}$), 181.7 (*C*NR, CNXyl), 137.8, 136.4, 136.3, 136.2, 134.1, 131.8, 129.6, 128.7, 128.3, 127.4, 125.8, 125.3, 21.3 (*p*-Mes), 20.6 (*o*-Mes), 19.3 (*C*H_3, Xyl) ppm. FTIR (C_6D_6, KBr windows, 25 ˚C): CNXyl ν_{CN} = 2116 (m) cm^{-1}, $CNAr^{Mes2}$ ν_{CN} = 2037 (s), 1977 (vs) cm^{-1} also, 3000 (b sh), 2955 (vw), 2919 (w), 2858 (w), 1612 (m), 1580 (m), 1462 (m), 1416 (m), 1374 (m), 1032 (w), 849 (m), 802 (vw), 782 (w), 769 (w), 755 (m), 738 (w), 668 (m), 602 (vw), 566 (vw) cm^{-1} (ν_{CoH} was not unambiguously located, presumably due to overlap with intense ν_{CN} stretches). Anal. Calcd. For $C_{84}H_{85}N_4Co$: C, 83.41; H, 7.08; N, 4.63. Found: C, 83.69; H, 6.99; N, 4.13.

S1.9. Synthesis of $HCo(CNAr^{Mes2})_3(PMe_3)$ (4^{PMe3}): $HCo(CNAr^{Mes2})_4$ (**1**, 0.050 g, 0.035 mmol) was dissolved in THF (15 mL) and allowed to stir for 5 min. To this reaction mixture, a THF solution of $P(Me)_3$ (0.003 g, 0.037 mmol, 2 mL, 1.05 equiv) was added. The resulting solution was allowed to stir at room temperature for 16 h. Thereafter, the reaction mixture was concentrated to a bright yellow solid under reduced pressure. The material was suspended in MeCN (5 mL) and filtered. The solid was washed with MeCN (3 x 3 mL), *n*-pentane (4 x 5 mL) and Et_2O (3 x 0.5 mL) to afford a bright yellow powder. Single crystals of $HCo(CNAr^{Mes2})_3(PMe_3)$ were obtained from a saturated MeCN solution at -30 ˚C. Yield: 0.022 g, 0.019 mmol, 54 %. ^{1}H NMR (400.1 MHz, C_6D_6, 20 ˚C): δ = 6.96-6.88 **(**m, 9H, *m*-Ph and *p*-Ph), 6.90 (s, 12H, *m*-Mes) 2.22 (s, 18H, *p*-Mes), 2.08 (s, 36H, *o*-Mes), 0.29 (d, 9H, $^2J_{PH}$ = 8.4 Hz, P(CH_3)$_3$), –11.51 (d, 1H, J_{PH} = 77 Hz, Co–*H*) ppm. $^{13}C\{^1H\}$ NMR (100.605 MHz, C_6D_6, 20 ˚C): δ = 182.2 (d, J_{PC} = 21 Hz, *C*NR), 137.5 (two peaks: 137.52, 137.51), 136.7 (two peaks: 136.69, 136.67), 136.4, 132.1, 129.7, 128.7, 124.7, 21.3 (*p*-Mes), 20.7 (*o*-Mes), 19.0 (d, $^1J_{PC}$ = 23 Hz, P(*C*H_3)$_3$) ppm. $^{31}P\{^1H\}$ NMR (121.47 MHz, C_6D_6, 20 ℃): δ = 12.76 (s, *P*Me_3) ppm. FTIR (C_6D_6, KBr windows, 25 ˚C): ν_{CN} = 2071 (sh), 2032 (m), 1952 (vs) cm^{-1}, also 2962 (m), 2918 (m), 2854 (w), 1613 (m), 1580 (m), 1416 (s), 950 (m), 850 (m), 800 (m), 755 (m), 652 (m) cm^{-1} (ν_{CoH} was not unambiguously located, presumably due to overlap with intense ν_{CN} stretches). Anal. Calcd. For $C_{78}H_{85}N_3PCo$: C, 81.15; H, 7.42; N, 3.64. Found C, 80.31; H, 7.14; N, 4.29.

S1.10. Synthesis of $HCo(CNAr^{Mes2})_3(PPh_3)$ (4^{PPh3}): $HCo(CNAr^{Mes2})_4$ (**1**, 0.075 g, 0.053 mmol) was dissolved in THF (15 mL) and allowed to stir for 5 min. To this reaction mixture, a THF solution of $P(Ph)_3$ (0.014 g, 0.054 mMol, 2 mL, 1.02 equiv.) was added. The resulting solution was allowed to stir at room temperature for 16 h. Thereafter, the reaction mixture was concentrated to a bright yellow solid under reduced pressure. The material was suspended in MeCN (5 mL) and filtered. The solid was washed with MeCN (3 x 3 mL), *n*-pentane (4 x 5 mL) and Et_2O (3 x 0.5 mL) to afford a bright yellow powder. Single crystals of $HCo(CNAr^{Mes2})_3(PPh_3)$ were obtained from a saturated MeCN solution at –30 ˚C. Yield: 30.1 mg, 0.022 mmol 41.5%. ^{1}H NMR (300.1 MHz, C_6D_6, 20 ˚C): δ = 7.03-6.97 (m, 12H, *o*-Ph and *m*-Ph, PPh_3), 6.89 (t, 3H, J = 7 Hz, *p*-Ph $CNAr^{Mes2}$), 6.80 (d, 6H, J = 7 Hz, *m*-Ph $CNAr^{Mes2}$), 6.73 (s, 12H, *m*-Mes), 6.70 (t, 3H, J = 7 Hz, *p*-Ph $P(Ph)_3$), 2.03 (s, 18H, *p*-Mes), 2.02 (s, 36H, *o*-Mes), –12.34 (d, 1H, J_{HP} = 44 Hz, hydride) ppm. $^{13}C\{^1H\}$ NMR (100.6 MHz, C_6D_6, 20 ℃): δ = 178.8 (*C*NR), 138.2 (d, $^1J_{CP}$ = 37 Hz, *i*-Ph, $P(Ph)_3$), 137.9 (two peaks: 137.90, 137.89), 136.2, 135.7 (two peaks: 135.73, 135.72), 135.6, 133.9 (d, $^2J_{CP}$ = 12 Hz, *o*-Ph, PPh_3), 129.8, 128.9, 127.4 (d, $^3J_{CP}$ = 9 Hz, *m*-Ph, PPh_3), 125.0, 21.4 (*o*-Mes), 21.2 (*p*-Mes) ppm. $^{31}P\{^1H\}$ NMR (121.47 MHz, C_6D_6, 20 ℃): δ = 61.05 (s, *P*Ph_3) ppm. FTIR (C_6D_6, KBr windows, 25 ˚C): ν_{CN} = 2074 (m), 2027 (m), 1968 (vs) cm^{-1} also, 3051 (vw), 2959 (m), 1610 (m), 1580 (m), 1415 (m), 1260 (m), 1113 (bm), 1027 (bm), 802 (w), 755 (w), 694 (w) cm^{-1}. Multiple attempts to obtain a satisfactory combustion analysis were unsuccessful.

S1.11. Synthesis of $HCo(CNAr^{Mes2})_3(CO)$ (4^{CO}): A resealable ampoule equipped with a side arm was charged with a C_6H_6 solution of $HCo(CNAr^{Mes2})_4$ (**1**, 1.00 g, 0.705 mmol, 100 mL). The solution was stirred for 5 m, frozen in liquid dinitrogen and the vessel evacuated to ~10 mTorr. The ampoule was then sealed and the side arm was fitted with a rubber septum. The sealed side arm was flushed with argon, evacuated and the ampule was opened. CO was then added via airfree syringe (17 mL, 0.0705 mmol, 1.0 equiv). The reaction mixture was allowed to rest in liquid dinitrogen for an additional 2 min to ensure all CO had condensed. The ampoule was resealed and allowed to warm to room temperature and react for 2 h. During this time, a color change from orange to bright yellow was observed. The reaction mixture was concentrated to a bright yellow solid under reduced pressure. It was then suspended in MeCN (5 mL) and filtered. The precipitate was then washed with MeCN (3 x 1 mL) and pentane (4 x 0.2 mL) to afford a bright yellow powder. Yield: 0.510 g, 0.045 mmol, 65.4%. Single crystals of $HCo(CNAr^{Mes2})_3CO$ were be obtained from a saturated MeCN solution at –30 ˚C. ^{1}H NMR (C_6D_6) and of the single crystals matched previously reported characterization data for $HCo(CNAr^{Mes2})_3(CO)$.[4]

S1.12. Synthesis of $Co(\kappa^1\text{-}C\text{-}C(H)NAr^{Mes2})(CNAr^{Mes2})_2(CO)_2$ (5): In an ampoule, $HCo(CNAr^{Mes2})_4$ (**1**; 0.060 g, 0.042 mmol) was dissolved in C_6H_6 (3 mL) and degassed by freeze-pump-thaw cycles. At room temperature, the reaction mixture was then treated with CO (1 atm) and stirred vigorously for 15 min. The reaction mixture was then frozen and the C_6H_6 was lyophilized. The resulting yellow solid was suspended in MeCN (5 mL) and filtered. The yellow solid was washed with MeCN (3 x 1 mL) and *n*-pentane (1 mL) to remove free $CNAr^{Mes2}$. It was then dissolved in a minimal amount of Et_2O, filtered and stored at –35 ˚C to afford yellow crystals which were collected and dried *in*

vacuo. Yield: 0.022 g, 0.020 mmol, 46.4 %. ^{1}H NMR (499.8 MHZ, C_6D_6, 20 ˚C): δ = 9.07 (s, 1H, (*H*)CNR), 7.00 (t, 2H, *J* = 7 Hz, *p*-Ph), 6.93 (s, 4H, *m*-Mes), 6.91-6.88 (m, 3H, *m*-Ph and *p*-Ph), 6.82 (s, 8H, *m*-Mes), 6.79 (d, 4H, *m*-Ph), 2.43 (s, 6H, *p*-Mes), 2.34 (s, 12H, *o*-Mes), 2.22 (s, 12H, *p*-Mes), 1.93 (s, 24H, *o*-Mes) ppm. ^{13}C{^{1}H} NMR (125.7 MHz, C_6D_6, 20 ˚C): δ = 197.3 (*C*O), 183.1 (H*C*NR), 172.1 (*C*NR), 153.4, 139.2, 138.2, 137.7, 136.1, 135.5, 135.1, 134.6, 132.1, 129.7, 129.4, 129.1, 128.8, 128.4, 128.3, 123.0, 21.6 (*p*-Mes), 21.5 (*o*-Mes), 21.4 (*p*-Mes), 20.5 (*o*-Mes) ppm. ^{13}C NMR (125.7 MHz, C_6D_6, 20 ˚C): δ = 183.1 (d, $^{1}J_{CH}$ = 148 Hz, H*C*NR). FTIR (C_6D_6; KBr Window; 20 ˚C): ν_{CN} = 2132 (s), 2032 (s) cm^{-1}, ν_{CO} = 2013 (vs), 1982 (vs) cm^{-1}, $\nu_{(H)\text{-}CNR}$ = 2857 (w) cm^{-1}, $\nu_{(H)C=NR}$ = 1561 (s) cm^{-1} also, 3001 (vw), 2970 (sh), 2920 (m), 1638 (w), 1614 (m) 1584 (m), 1460 (w), 1440 (w), 1415 (w), 1376 (w), 1279 (w), 1257 (w), 1183 (w), 1030 (vw), 849 (m), 755 (w), 604 (w), 552 (m) cm^{-1}. HRMS: m/z Calcd: 1134.5326; m/z Found: 1134.5342. Anal. Calcd. For $C_{77}H_{76}CoN_3O_2$: C, 81.53; H, 6.75; N, 3.70. Found: C, 79.79; H, 6.68; N, 3.80.

S1.13. Synthesis of Co(κ^{1}-*C*-C[C(H)NAr^{Mes2}]NAr^{Mes2})(CNAr^{Mes2})(CO)$_3$ (6): In a resealable ampoule, HCo(CNAr^{Mes2})$_4$ (**1**; 0.100 g, 0.071 mmol) was dissolved in THF (10 mL) and degassed. The reaction mixture was then placed under one atmosphere of CO and allowed to stir for 18 h. The reaction mixture was concentrated to a yellow-solid under reduced pressure, suspended in MeCN (20 mL) and filtered. The yellow solid was then washed with MeCN (3 x 10 mL) to remove free CNAr^{Mes2}. It was then dissolved in a minimal amount of Et_2O, filtered and stored at –35 ˚C. Yellow crystals were collected and dried *in vacuo*. Yield 0.047 g, 0.040 mmol, 56.9 %. ^{1}H NMR (499.8 MHz, C_6D_6, 20 ˚C): δ = 7.21 (s, 1H, RNC(*H*)CNR), 7.08-7.05 (m, 3H, Ar), 6.97 (t, 1H, *J* = 7 Hz, *p*-Ph), 6.98-6.95 (m, 10H, Ar), 6.83 (s, 4H, *m*-Mes), 6.80 (br s, 2H, Ar), 6.78 (d, 2H, *J* = 7 Hz, *m*-Ph), 2.37 (s, 6H, C*H*$_3$), 2.34 (s, 6H, C*H*$_3$), 2.32 (s, 6H, C*H*$_3$), 2.31 (s, 6H, C*H*$_3$), 2.13 (s, 6H, C*H*$_3$), 2.04 (s, 12H, C*H*$_3$), 1.98 (s, 12H, *o*-Mes) ppm. ^{13}C{^{1}H} NMR (125.7 MHz, C_6D_6, 20 ˚C): δ = 194.2 (RNC(H)=*C*NR), 185.4 (*C*O), 167.3 (RN*C*(H)=CNR), 163.6 (*C*NR), 152.1, 149.0, 139.1, 138.1, 137.3, 137.2, 136.8, 136.0, 135.9, 135.5, 135.4, 135.3, 133.7, 132.9, 130.6, 130.5, 129.9, 129.3, 129.4, 129.3, 129.0, 128.8, 128.4, 128.3, 125.2, 123.8, 21.6, 21.5, 21.4, 21.3, 21.2, 20.8, 20.2 ppm. FTIR (C_6D_6; KBr Window; 20 ˚C): ν_{CN} = 2154 (s), ν_{CO} = 2011 (vs), 2002 (s), 1985 (vs), cm^{-1} also, 3008 (sh), 2973 (w), 2920 (w), 2859 (w), 1638 (m), 1613 (m), 1578 (w), 1570 (w), 1456 (m), 1376 (w), 1332 (w), 1215 (m), 1205 (m), 1163 (sh), 1148 (m), 1117 (m), 847 (m), 760 (w), 682 (m), 601 (w) cm^{-1}. Anal. Calcd. For $C_{78}H_{76}CoN_3O_3$: C, 80.60; H, 6.59; N, 3.61. Found: C, 80.32; H, 6.77; N, 3.59.

S1.14. Synthesis of 1,1-H$_2$C=NAr^{Mes2} (7): A 350 mL re-sealable ampoule was charged with a stir bar and a C_6H_6 solution of HCo(CNAr^{Mes2})$_4$ (**1**; 0.040 g, 0.028 mmol, 4 mL). The ampoule was degassed using three freeze-pump-thaw cycles and pressurized with H_2 (1 atm). The reaction mixture was allowed to react for 12 h where it was then concentrated to a solid under reduced pressure. The solid residue was then extracted with C_6H_6 (10 mL) and passed through a plug packed with basic alumina then a plug packed with Celite. The resulting filtrate was concentrated to a solid under reduced pressure. The solid-was dissolved in a minimal amount of Et_2O and stored at –40 ˚C. Single colorless crystals were then collected and dried *in vacuo*. *Note*: H$_2$C=NAr^{Mes2} is extremely

moisture sensitive and will readily hydrolyze to afford H_2CO and H_2NAr^{Mes2}. Yield: 0.022 g, 0.065 mmol, 58 %. ^{1}H NMR (C_6D_6) ^{1}H NMR (499.8 MHz, C_6D_6, 20 ˚C): δ = 7.04 (t, 1H, *J* = 7 Hz, *p*-Ph), 6.99 (d, 2H, *J* = 7 Hz, *m*-Ph), 6.85 (s, 4H, *m*-Mes), 6.72 (d, 1H, $^1J_{HH}$ = 18 Hz, H_2C=NR), 6.41 (d, 1H, $^1J_{HH}$ = 18 Hz, H_2C=NR), 2.19 (s, 6H, *p*-Mes), 2.14 (s, 12H, *o*-Mes) ppm. $^{13}C\{^1H\}$ NMR (125.7 MHz, C_6D_6, 20 ˚C): δ = 153.4 (H_2C=NR), 137.1, 136.9, 136.5, 136.1, 131.9, 129.5, 128.7, 125.1, 21.2 (*p*-Mes), 21.0 (*o*-Mes) ppm. A proton coupled ^{13}C NMR was recorded to confirm the H_2C=NAr^{Mes2} formulation and provide coupling constants for the methyleneimine resonance. ^{13}C NMR (125.7 MHz, C_6D_6, 20 ˚C): δ = 153.4 (dd, $^1J_{CH}$ = 160 Hz, $^1J_{CH}$ = 180 Hz, H_2CNR) ppm. FTIR (C_6D_6; KBr Window; 20 ˚C): $\nu_{H2C=NR}$ =1605 (s) cm^{-1} also, 3012 (w, sh), 2959 (w), 2920 (m), 2856 (w), 1613 (w, sh), 1449 (s), 1377 (w), 1261 (w), 1071 (vw), 1041 (w), 1005 (vw), 852 (m), 794 (w), 750 (m), 680 (vw), 630 (vw), 567 (vw), 550 (vw) cm^{-1}. HRMS (ESI, THF): m/z Calcd for $[C_{25}H_{28}N]^+$: 342.2216; m/z Found: 342.2218.

S1.15. Catalytic Preparation of 1,1-H_2C=NAr^{Mes2} (7) from $HCo(CNAr^{Mes2})_4$ (1) and H_2: A 350 mL resealable ampoule was charged with a stir bar, $CNAr^{Mes2}$ (0.070 g, 0.206 mmol), C_6H_6 (5 mL) and $HCo(CNAr^{Mes2})_4$ (0.014 g, 0.010 mmol, 5 mol %). The ampoule was degassed using three freeze-pump-thaw cycles and pressurized with H_2 (1 atm). The reaction mixture was allowed to react for 15 h at room temperature where it was then concentrated to a solid under reduced pressure. ^{1}H NMR spectroscopy confirmed conversion of $CNAr^{Mes2}$ to 1,1-H_2C=NAr^{Mes2}. Percent conversion information is detailed for three trials in Table S1.1.

Table S1.1. Percent conversion data for the 1,1-hydrogenation of $CNAr^{Mes2}$ to 1,1-H_2C=NAr^{Mes2}, using 5 mol % $HCo(CNAr^{Mes2})_4$ with H_2 (1 atm), 15 h, RT.

	% Conversion of $CNAr^{Mes2}$ to 1,1-H_2C=NAr^{Mes2}
Trial 1	87 %
Trial 2	79 %
Trial 3	61 %
Average	76 ± 13 %

S1.16. $^{13}CNAr^{Mes2}$ Incorporation into Co(η^6-(Mes)-κ^1-*C*-C(H)NAr^{Mes2})(CNAr^{Mes2}) (2) and Co(η^6-(Mes)-κ^1-*C*-C[C(H)NAr^{Mes2}]NAr^{Mes2})(CNAr^{Mes2}): A pure sample of (**2**) (0.010 g, 0.014 mmol) was dissolved in C_6D_6 (~ 0.75 mL) and combined in a re-sealable NMR tube with 1.05 equiv $^{13}CNAr^{Mes2}$. The resulting reaction mixture was heated to 40 ˚C and analyzed by $^{13}C\{^1H\}$ NMR. The resulting spectrum showed incorporation of the ^{13}C label at both the terminal isocyanide and iminoformyl carbon positions (Figure S1.9). *Note*: The terminal isocyanide carbon in **2** is isochronous with free $CNAr^{Mes2}$. However, $^1J_{CH}$ (213 Hz) and $^3J_{CH}$ (18 Hz) coupling between the iminoformyl proton and both the iminoformyl and terminal isocyanide carbons could be observed and gave rise to a doublet of doublets (Figure S1.10). Thereafter, the reaction mixture was heated to 60 ˚C for 104 h and analyzed by $^{13}C\{^1H\}$ NMR. The resulting spectrum showed incorporation of the ^{13}C label at both of the diimine carbon positions and the terminal isocyanide (Figure S1.11).

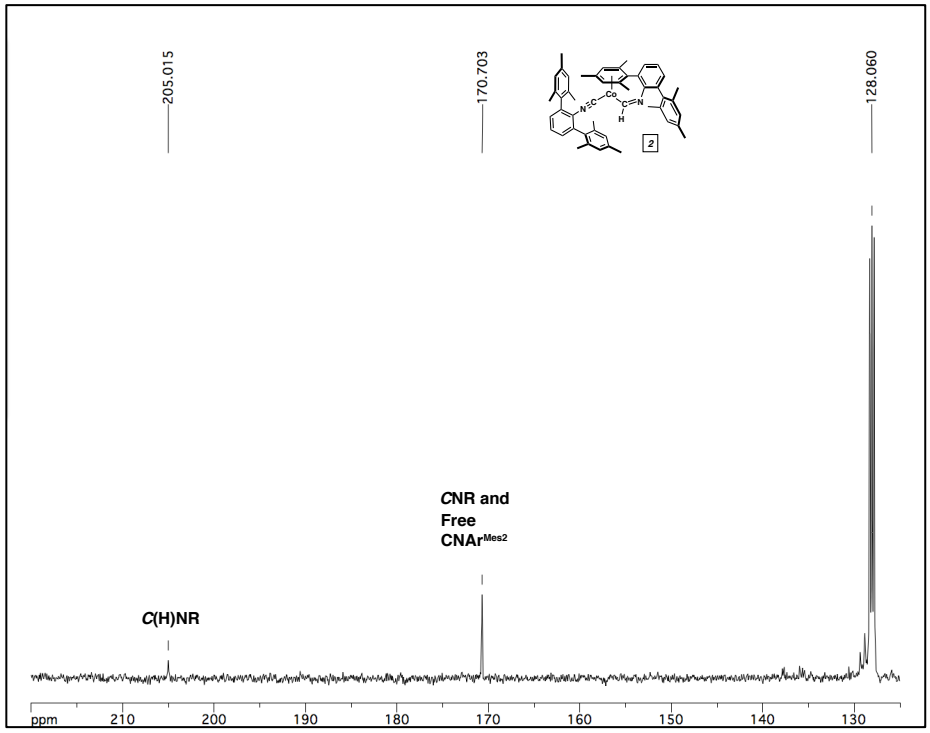

Figure S1.9. Isocyanide/iminoformyl region of the $^{13}C\{^1H\}$ NMR spectrum (125.7 MHz) of Co(η^6-(Mes)-κ^1-*C*-C(H)NAr^{Mes2})(CNAr^{Mes2}) (2) after 1 h at 40 ˚C in the presence of $^{13}CNAr^{Mes2}$.

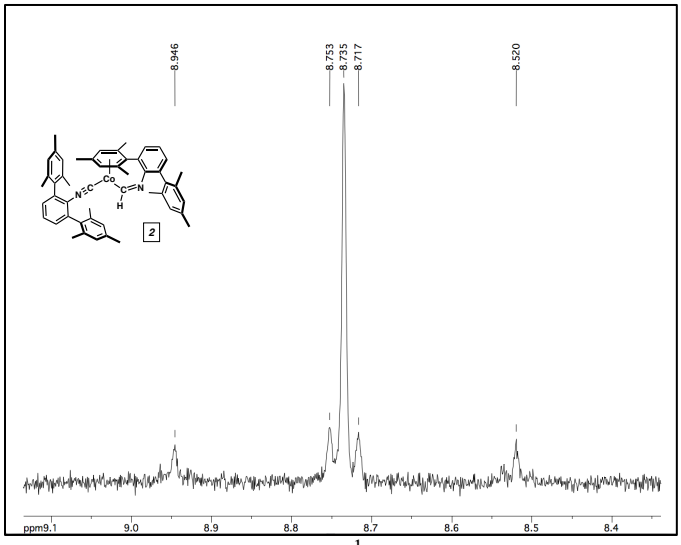

Figure S1.10. Enlarged view of iminoformyl ^{1}H NMR resonance (500.0 MHz) for Co(η^6-(Mes)-κ^1-*C*-C(H)NAr^{Mes2})(CNAr^{Mes2}) (**2**) after 15 h at 40 ˚C in the presence of ^{13}CNAr^{Mes2}. Similar spectral features are visible after 1 h but are less well resolved. Coupling constants were measured to be $^{1}J_{CH}$ (213 Hz) and $^{3}J_{CH}$ (18 Hz).

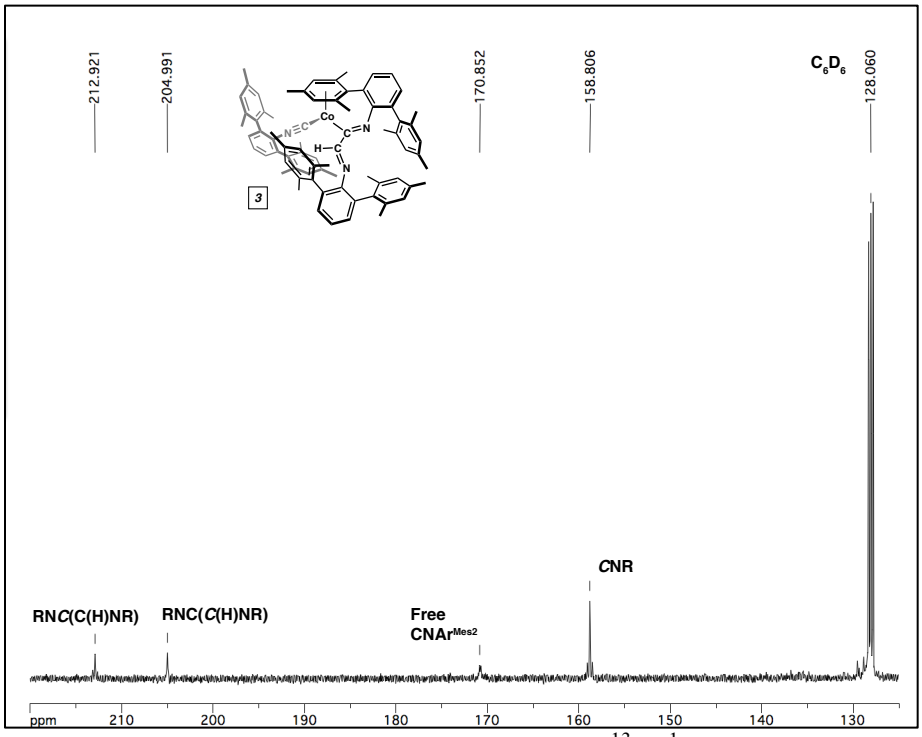

Figure S1.11. Isocyanide/iminoformyl region of the ^{13}C{^{1}H} NMR spectrum (125.7 MHz) of Co(η^6-(Mes)-κ^1-*C*-C(H)NAr^{Mes2})(CNAr^{Mes2}) (**2**) after 104 h at 60 ˚C in the presence of ^{13}CNAr^{Mes2}. Material has been completely converted to Co(η^6-(Mes)-κ^1-*C*-C[C(H)NAr^{Mes2}]NAr^{Mes2})(CNAr^{Mes2}) (**3**) with isotopic enrichment at the terminal isocyanide and both diimine carbon positions.

S2. Kinetic Studies on the Rate of $HCo(CNAr^{Mes2})_4$ Decay

S2.1 General Considerations and Experimental Methodology Time-Dependent Monitoring of $HCo(CNAr^{Mes2})_4$ and $DCo(CNAr^{Mes2})_4$ Decay: All time-dependent ^1H NMR measurements were recorded in a resealable J-Young tube on a JEOL ECA 500 NMR spectrometer equipped with a variable temperature controller. Samples of $HCo(CNAr^{Mes2})_4$ were prepared in a dinitrogen filled glovebox as C_6D_6 solutions (2.8 mM or 1.6 mM) with Cp_2Fe (3.9 mM) as internal standard. In a typical experiment, a solution was inserted into the NMR probe at room temperature. The instrument was then tuned, locked and shimmed. Thereafter, the probe was warmed to specified experimental temperature and allowed to equilibrate for exactly 5 minutes for temperatures 50 ˚C and below. At temperatures above 50 ˚C, the equilibration time was reduced to 2 minutes to account for the shorten half-lives at high temperatures. Single-pulse NMR acquisitions were employed in all experiments. Raw intensity data was obtained by integration of the *ortho*-mesityl C*H*$_3$ resonance in $HCo(CNAr^{Mes2})_4$ and calibrated using the intensity of the internal Cp_2Fe standard.

Ligand Inhibition Experiments: The rate of $HCo(CNAr^{Mes2})_4$ decay in the presence of additional $CNAr^{Mes2}$ was determined using the same methodology as detailed above with stock solutions containing $HCo(CNAr^{Mes2})_4$ (2.8 mM), $CNAr^{Mes2}$ (14 mM, 5.0 equiv) and Cp_2Fe (3.9 mM) as an internal standard. Stock solutions were prepared immediately prior to data acquisition.

Estimation of k_{obs} and Data Fitting for $HCo(CNAr^{Mes2})_4$ Decay Data: Estimates of k_{obs} for the decay of $HCo(CNAr^{Mes2})_4$ (**1**) were obtained from a non-linear least squares fit to the following function:

$$I(t) = (I_o - I_\infty)e^{-K_{obs}t} + I_\infty$$

Note: I_∞ = residual intensity at t = ∞, I_o = initial intensity. The terms I_∞, (I_o-I_∞), and k_{obs} are adjustable parameters optimized by least squares fitting.

To avoid potential biases arising from non-linear weighting introduced by fitting to first-order plots (e.g., ln[concentration] vs. time plots), the value of k_{obs} was estimated using non-linear least squares fitting methodology. A residual intensity term, I_∞, was included to account for partial overlap of integrated resonances. In all instances, it was found that (I_o-I_∞) >> I_∞. This provides further evidence that the decay of $HCo(CNAr^{Mes2})_4$ (**1**) is appropriately modeled as first-order in [**1**].

S2.2. Determination of 1st Order Decay in [HCo(CNAr^{Mes2})$_4$] ([1]) using 2.8 and 1.6 mM C_6D_6 Solutions at 40 ˚C.

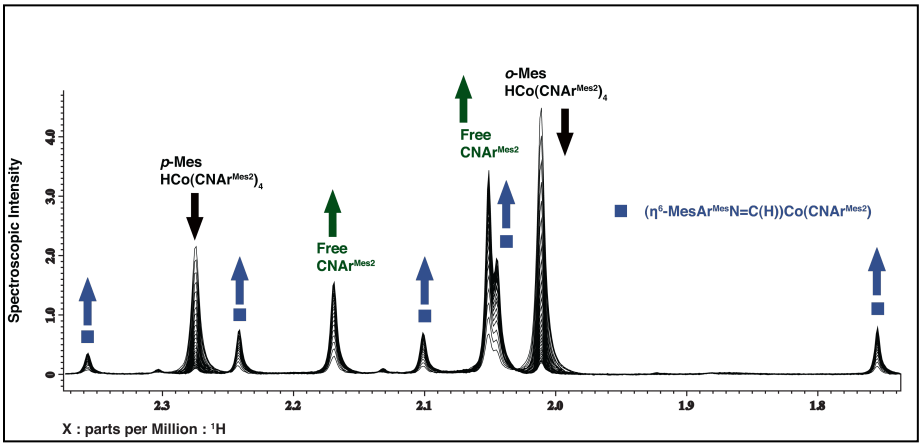

Figure S2.1. Representative stack plot for the decay of 2.8 mM HCo(CNAr^{Mes2})$_4$ (**1**) solutions at 40 ˚C in C_6D_6. Arrows indicate direction of peak intensity change over time.

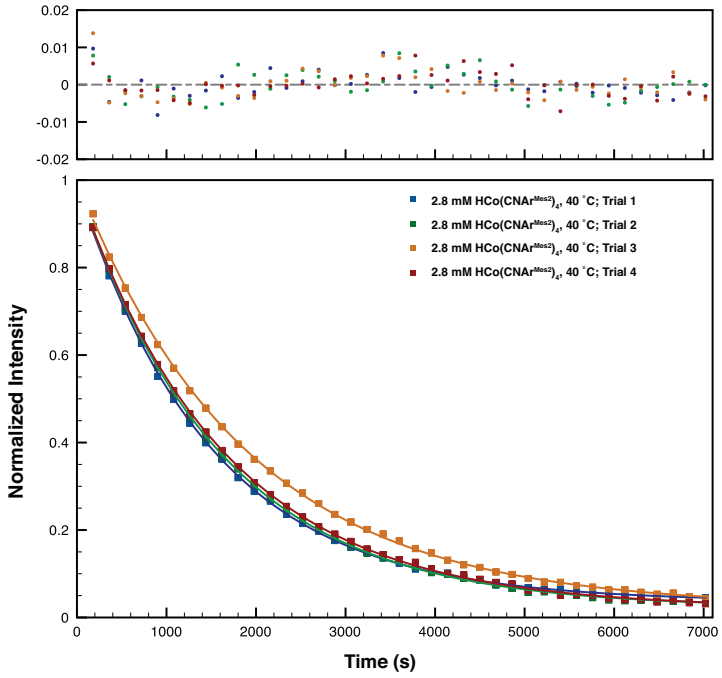

Figure S2.2. Decay of 2.8 mM HCo(CNAr^{Mes2})$_4$ (**1**) solutions at 40˚C in C_6D_6. Bottom: Normalized intensity vs. time with non-linear least squares fit (4 trials). Top: Plot of residuals from the difference between observed experimental intensity and the predicted intensity obtained from non-linear least squares fitting.

Table S2.1. Measured k_{obs} for the decay of 2.8 mM C_6D_6 solutions of $HCo(CNAr^{Mes2})_4$ (**1**) at 40 ˚C. Rate estimates were determined from a non-linear least squares best fit of [**1**] vs. time.

Time Interval 180-7020 seconds	k_{obs} (s^{-1})	Error	R^2
2.8 mM 40 ˚C Trial 1	6.7×10^{-4}	4.0×10^{-6}	0.999
2.8 mM 40 ˚C Trial 2	6.3×10^{-4}	4.2×10^{-6}	0.999
2.8 mM 40 ˚C Trial 3	5.3×10^{-4}	2.7×10^{-6}	0.999
2.8 mM 40 ˚C Trial 4	6.1×10^{-4}	3.0×10^{-6}	0.999
	Average k_{obs} (s^{-1})	St. Dev (σ)	–
Average	6.1×10^{-4}	5.8×10^{-5}	–

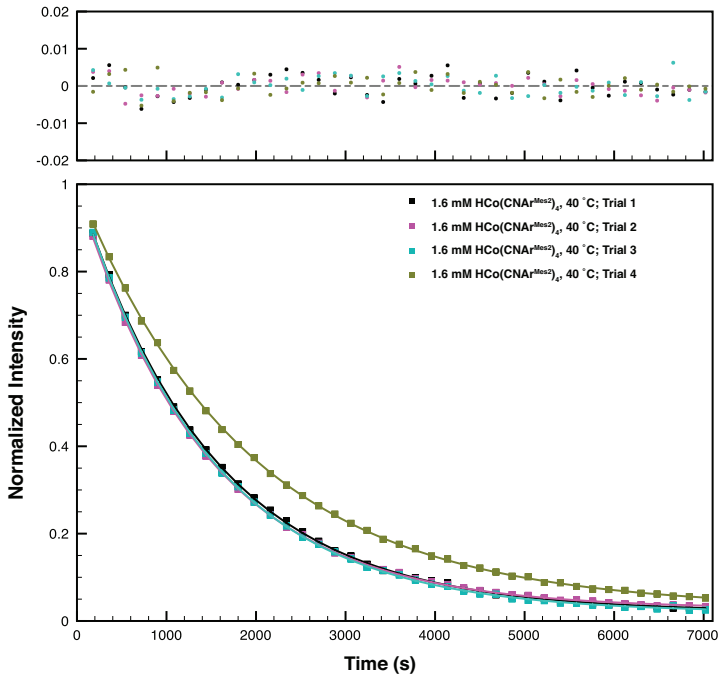

Figure S2.3. Decay of 1.6 mM $HCo(CNAr^{Mes2})_4$ (**1**) at 40˚C in C_6D_6. Bottom: Normalized intensity vs. time with non-linear least squares fit (4 trials). Top: Plot of residuals from the difference between observed experimental intensity and the predicted intensity obtained from non-linear least squares fitting.

Table S2.2. Measured k_{obs} for the decay of 1.6 mM C_6D_6 solutions of $HCo(CNAr^{Mes2})_4$ (**1**) at 40˚C. Rate estimates were determined from a non-linear least squares best fit of [**1**] vs. time.

Time Interval 180-7020 seconds	k_{obs} (s^{-1})	Error	R^2
1.6 mM 40 ˚C Trial 1	$6.7x10^{-4}$	$3.3x10^{-6}$	0.999
1.6 mM 40 ˚C Trial 2	$7.0x10^{-4}$	$2.8x10^{-6}$	0.999
1.6 mM 40 ˚C Trial 3	$6.9x10^{-4}$	$3.0x10^{-6}$	0.999
1.6 mM 40 ˚C Trial 4	$5.3x10^{-4}$	$2.5x10^{-6}$	0.999
	Average k_{obs} (s^{-1})	St. Dev (σ)	–
Average	$6.5x10^{-4}$	$7.9x10^{-5}$	–

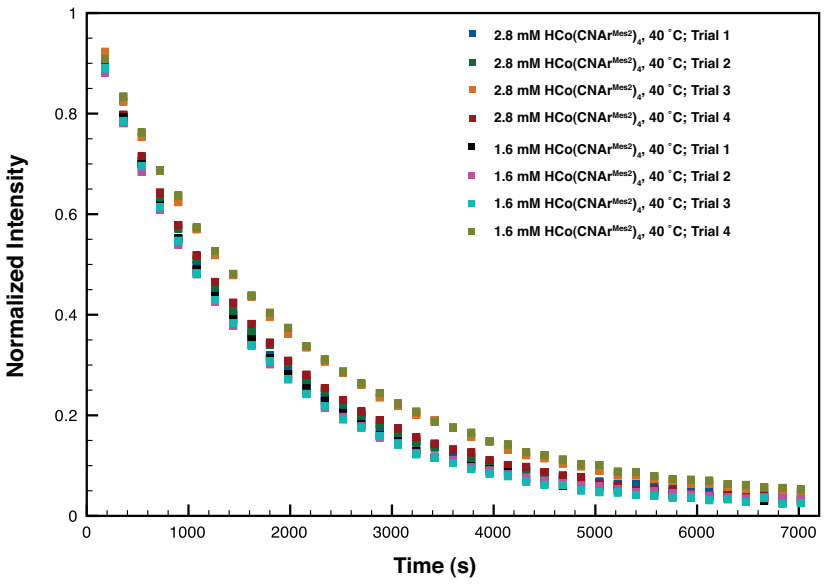

Figure S2.4. Decay of 1.6 mM and 2.8mM $HCo(CNAr^{Mes2})_4$ (**1**) at 40 ˚C in C_6D_6. Normalized intensity vs. time.

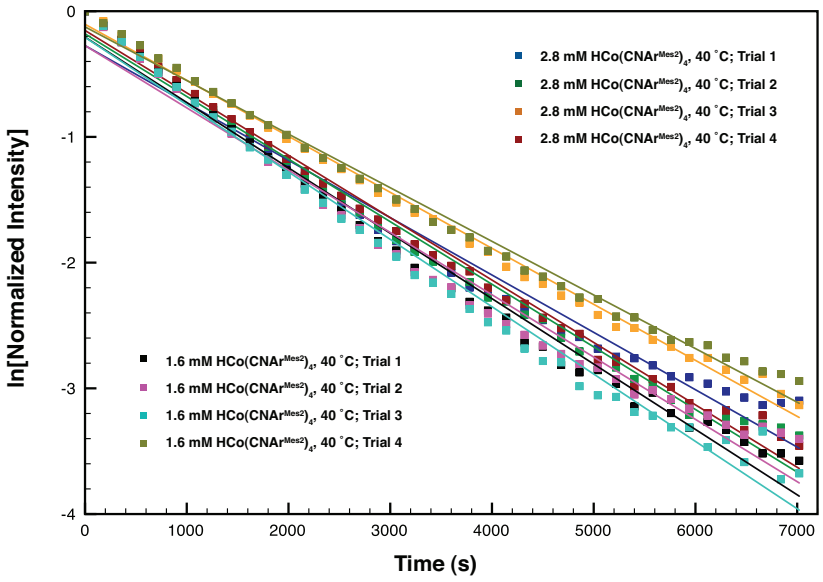

Figure S2.5. Normalized ln[intensity] vs. time plot for the decay of 1.6 mM and 2.8 mM solutions of $HCo(CNAr^{Mes2})_4$ (**1**) at 40˚C in C_6D_6. Linear fits to ln[**1**] vs. time suggest the decay of $HCo(CNAr^{Mes2})_4$ (**1**) is first-order in [**1**]. Changing the concentration of **1** by a factor of 1.75 shows no observable change in the slope of ln[**1**] vs. time.

Table S2.3. Average measured k_{obs} for the decay 1.6 mM and 2.8 mM C_6D_6 solutions of $HCo(CNAr^{Mes2})_4$ (**1**) at 40 ˚C. Changing the concentration by a factor of 1.75 affords average K_{obs} values that are the same, within error, suggesting the decay of $HCo(CNAr^{Mes2})_4$ (**1**) is independent of initial $HCo(CNAr^{Mes2})_4$ (**1**) concentration and consistent with first-order behavior in [**1**].

Time Interval 180-7020 seconds	Average k_{obs} (s^{-1})	St. Dev (σ)
2.8 mM 40 ˚C (4 Trials)	6.1×10^{-4}	5.8×10^{-5}
1.6 mM 40 ˚C (4 Trials)	6.5×10^{-4}	7.9×10^{-5}

S2.3 Kinetic Isotope Effect (KIE) Determination using 2.8 mM C_6D_6 Solutions of $HCo(CNAr^{Mes2})_4$ and $DCo(CNAr^{Mes2})_4$ at 40 ˚C.

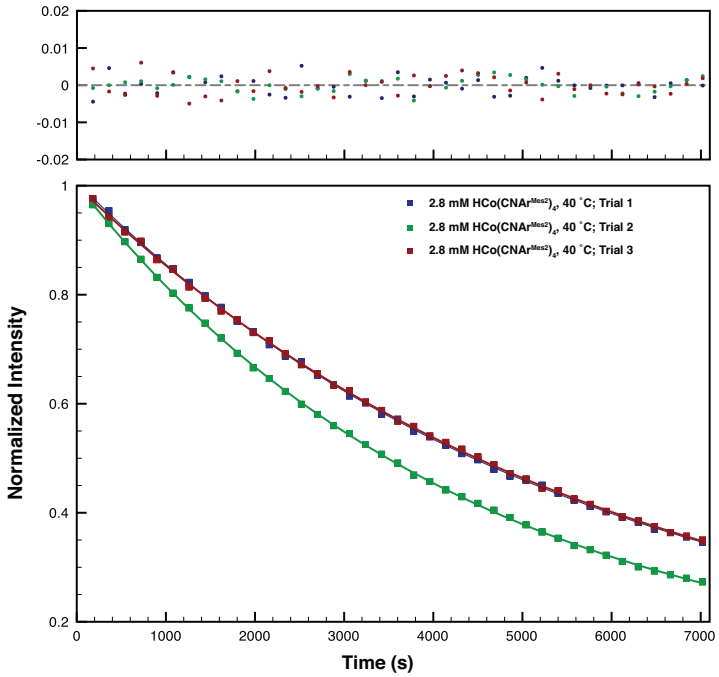

Figure S2.6. Decay of 2.8 mM $DCo(CNAr^{Mes2})_4$ (**1-*d*$_1$**) at 40˚C in C_6D_6. Bottom: Normalized intensity vs. time with non-linear least squares fit (3 trials). Top: Plot of residuals from the difference between observed experimental intensity and the predicted intensity obtained from non-linear least squares fitting.

Table S2.4. Measured k_{obs} for the decay of 2.8 mM C_6D_6 solutions of $DCo(CNAr^{Mes2})_4$ (**1-*d*$_1$**) at 40˚C. Rate estimates were determined from a non-linear least squares best fit of [**1-*d*$_1$**] vs. time.

Time Interval 180-7020 seconds	k_{obs} (s^{-1})	Error	R^2
2.8 mM 40 ˚C Trial 1	1.8×10^{-4}	2.5×10^{-6}	0.999
2.8 mM 40 ˚C Trial 2	2.3×10^{-4}	1.8×10^{-6}	0.999
2.8 mM 40 ˚C Trial 3	1.7×10^{-4}	2.8×10^{-6}	0.999
	Average k_{obs} (s^{-1})	St. Dev (σ)	–
Average	1.9×10^{-4}	3.1×10^{-5}	–

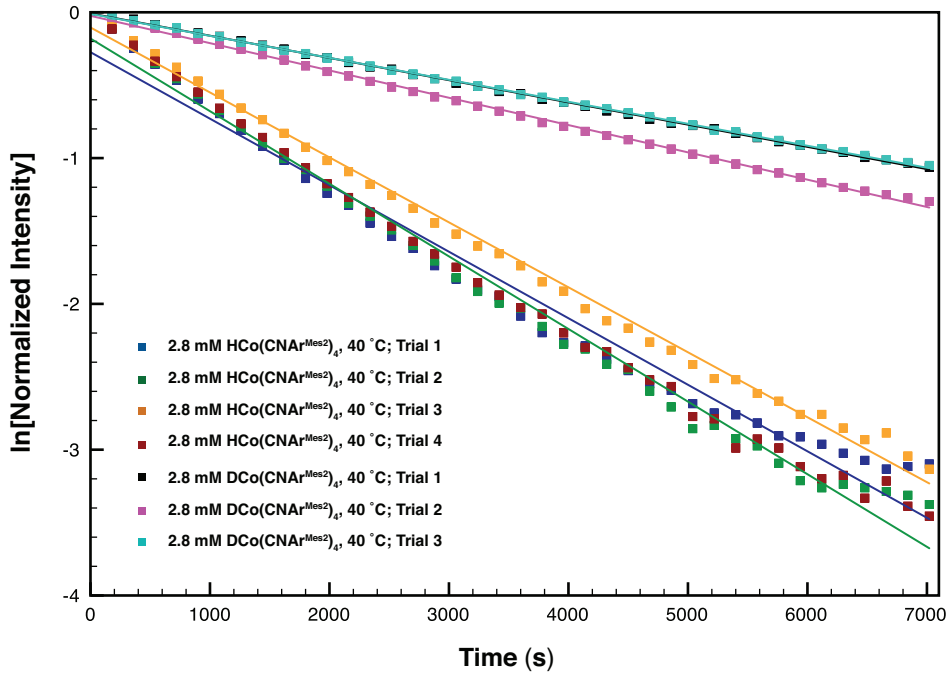

Figure S2.7. Normalized ln[intensity] vs. time plot for 2.8 mM solutions of $DCo(CNAr^{Mes2})_4$ (**1-*d*$_1$**) and $HCo(CNAr^{Mes2})_4$ at 40 ˚C in C_6D_6.

Table S2.5. Kinetic isotope effect for 2.8 mM C_6D_6 solutions of $HCo(CNAr^{Mes2})_4$ (**1**) and $DCo(CNAr^{Mes2})_4$ (**1-*d*$_1$**) at 40˚C.

Time Interval 180-7020 seconds	Average k_{obs} (s^{-1})	St. Dev (σ)
$HCo(CNAr^{Mes2})_4$ 2.8 mM 40 ˚C (4 Trials)	6.1×10^{-4}	5.8×10^{-5}
$DCo(CNAr^{Mes2})_4$ 2.8 mM 40 ˚C (4 Trials)	1.9×10^{-4}	3.1×10^{-5}
	k_H/k_D	Error
Isotope Effect	3.2	0.59

S2.4 Estimation of k_{obs} for 2.8 mM C_6D_6 Solutions of $HCo(CNAr^{Mes2})_4$ Decay at 5 ˚C Increments Between 60 ˚C and 25 ˚C.

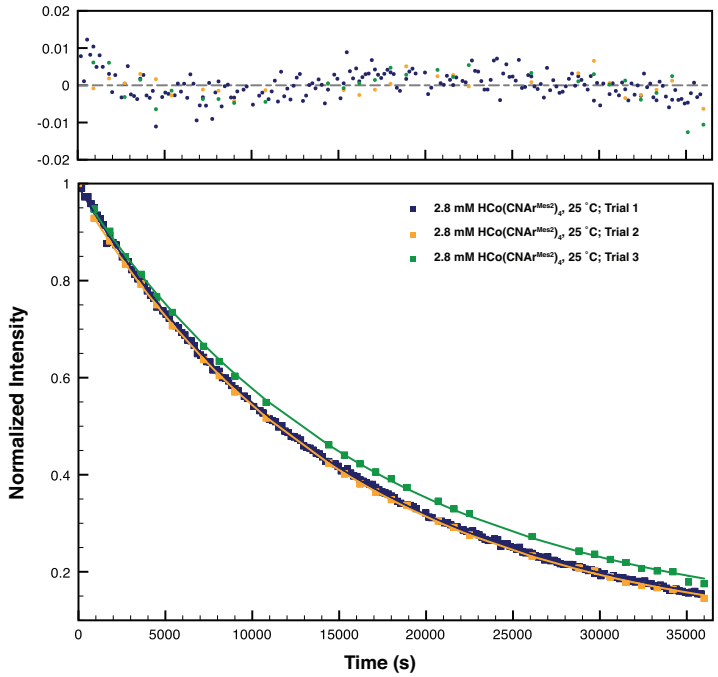

Figure S2.8. Decay of 2.8 mM $HCo(CNAr^{Mes2})_4$ (**1**) at 25 ˚C in C_6D_6. Bottom: Normalized intensity vs. time with non-linear least squares fit (3 trials). Top: Plot of residuals from the difference between observed experimental intensity and the predicted intensity obtained from non-linear least squares fitting.

Table S2.6. Measured k_{obs} for the decay of 2.8 mM solutions of $HCo(CNAr^{Mes2})_4$ (**1**) at 25 ˚C in C_6D_6. Rate estimates were determined from a non-linear least squares best fit of [**1**] vs. time.

Time Interval 0-36000 seconds	k_{obs} (s^{-1})	Error	R^2
2.8 mM 25 ˚C Trial 1	6.6×10^{-5}	3.1×10^{-7}	0.999
2.8 mM 25 ˚C Trial 2	6.5×10^{-5}	3.9×10^{-7}	0.999
2.8 mM 25 ˚C Trial 3	6.1×10^{-5}	5.9×10^{-7}	0.999
	Average k_{obs} (s^{-1})	St. Dev (σ)	–
Average	6.4×10^{-5}	2.5×10^{-6}	–

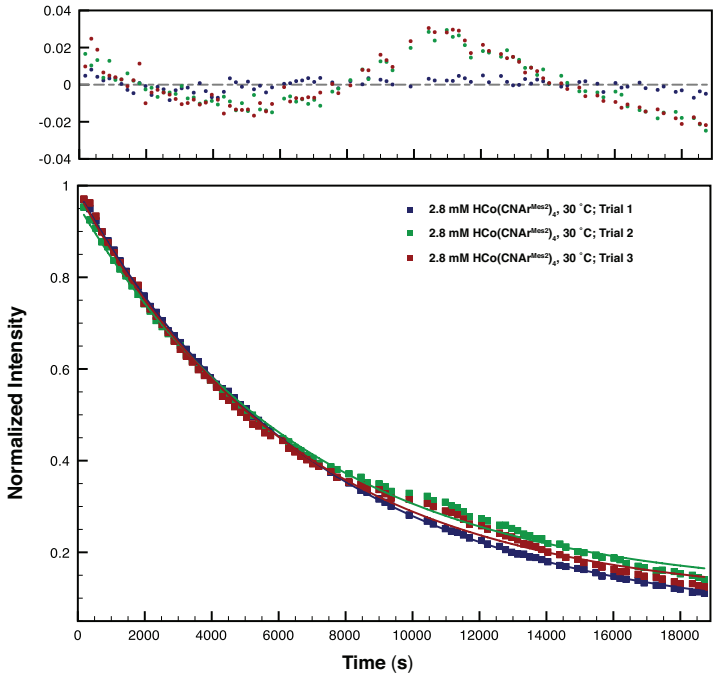

Figure S2.9. Decay of 2.8 mM $HCo(CNAr^{Mes2})_4$ (**1**) at 30 ˚C in C_6D_6. Bottom: Normalized intensity vs. time with non-linear least squares fit (3 trials). Top: Plot of residuals from the difference between observed experimental intensity and the predicted intensity obtained from non-linear least squares fitting.

Table S2.7. Measured k_{obs} for the decay of 2.8 mM solutions of $HCo(CNAr^{Mes2})_4$ (**1**) at 30 ˚C in C_6D_6. Rate estimates were determined from a non-linear least squares best fit of [**1**] vs. time.

Time Interval 180-18720 seconds	k_{obs} (s^{-1})	Error	R^2
2.8 mM 30 ˚C Trial 1	$1.4x10^{-4}$	$7.0x10^{-7}$	0.999
2.8 mM 30 ˚C Trial 2	$1.5x10^{-4}$	$1.5x10^{-6}$	0.999
2.8 mM 30 ˚C Trial 3	$1.5x10^{-4}$	$1.x10^{-6}$	0.999
	Average k_{obs} (s^{-1})	St. Dev (σ)	–
Average	$1.5x10^{-4}$	$6.1x10^{-6}$	–

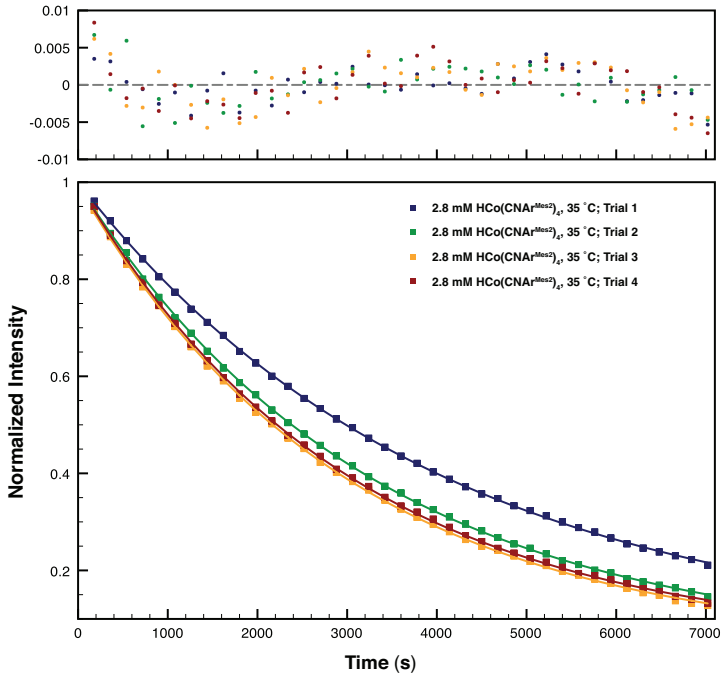

Figure S2.10. Decay of 2.8 mM $HCo(CNAr^{Mes2})_4$ (**1**) at 35 ˚C in C_6D_6. Bottom: Normalized intensity vs. time with non-linear least squares fit (4 trials). Top: Plot of residuals from the difference between observed experimental intensity and the predicted intensity obtained from non-linear least squares fitting.

Table S2.8. Measured k_{obs} for the decay of 2.8 mM solutions of $HCo(CNAr^{Mes2})_4$ (**1**) at 35 ˚C in C_6D_6. Rate estimates were determined from a non-linear least squares best fit of [**1**] vs. time.

Time Interval 180-7020 seconds	K_{obs} (s^{-1})	Error	R^2
2.8 mM 35 ˚C Trial 1	$2.5x10^{-4}$	$1.98x10^{-6}$	0.999
2.8 mM 35 ˚C Trial 2	$3.1x10^{-4}$	$2.3x10^{-6}$	0.999
2.8 mM 35 ˚C Trial 3	$3.4x10^{-4}$	$2.8x10^{-6}$	0.999
2.8 mM 35 ˚C Trial 4	$3.4x10^{-4}$	$2.7x10^{-6}$	0.999
	Average K_{obs} (s^{-1})	St. Dev (σ)	–
Average	$3.1x10^{-4}$	$4.0x10^{-5}$	–

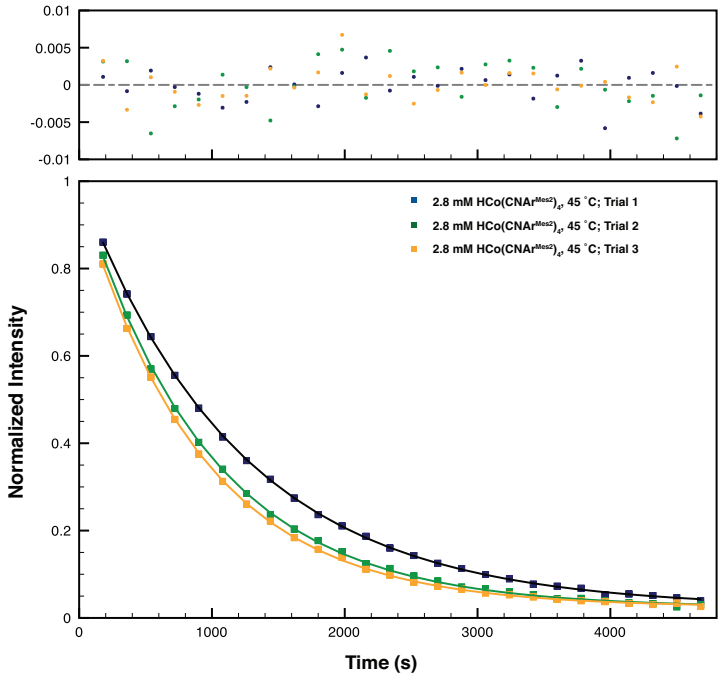

Figure S2.11. Decay of 2.8 mM HCo(CNAr^{Mes2})$_4$ (**1**) at 45 ˚C in C_6D_6. Bottom: Normalized intensity vs. time with non-linear least squares fit (3 trials). Top: Plot of residuals from the difference between observed experimental intensity and the predicted intensity obtained from non-linear least squares fitting.

Table S2.9. Measured k_{obs} for the decay of 2.8 mM solutions of HCo(CNAr^{Mes2})$_4$ (**1**) at 45 ˚C in C_6D_6. Rate estimates were determined from a non-linear least squares best fit of [**1**] vs. time.

Time Interval 180-4680 seconds	k_{obs} (s^{-1})	Error	R^2
2.8 mM 45 ˚C Trial 1	8.4×10^{-4}	3.7×10^{-6}	0.999
2.8 mM 45 ˚C Trial 2	1.0×10^{-3}	7.8×10^{-6}	0.999
2.8 mM 45 ˚C Trial 3	1.1×10^{-3}	6.0×10^{-6}	0.999
	Average k_{obs} (s^{-1})	St. Dev (σ)	–
Average	9.9×10^{-4}	1.4×10^{-4}	–

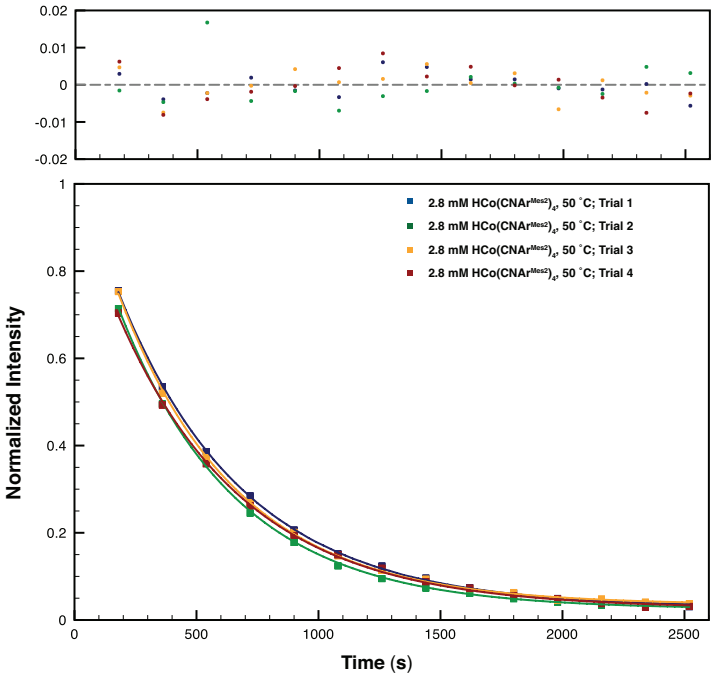

Figure S2.12. Decay of 2.8 mM HCo(CNAr^{Mes2})$_4$ (**1**) at 50 ˚C in C_6D_6. Bottom: Normalized intensity vs. time with non-linear least squares fit (4 trials). Top: Plot of residuals from the difference between observed experimental intensity and the predicted intensity obtained from non-linear least squares fitting.

Table S2.10. Measured k_{obs} for the decay of 2.8 mM solutions of HCo(CNAr^{Mes2})$_4$ (**1**) at 50 ˚C in C_6D_6. Rate estimates were determined from a non-linear least squares best fit of [**1**] vs. time.

Time Interval 180-2520 seconds	k_{obs} (s^{-1})	Error	R^2
2.8 mM 50 ˚C Trial 1	1.9×10^{-3}	2.2×10^{-5}	0.999
2.8 mM 50 ˚C Trial 2	2.1×10^{-3}	4.2×10^{-5}	0.999
2.8 mM 50 ˚C Trial 3	2.1×10^{-3}	4.0×10^{-5}	0.999
2.8 mM 50 ˚C Trial 4	1.9×10^{-3}	3.5×10^{-5}	0.999
	Average k_{obs} (s^{-1})	St. Dev (σ)	–
Average	2.0×10^{-3}	8.0×10^{-5}	–

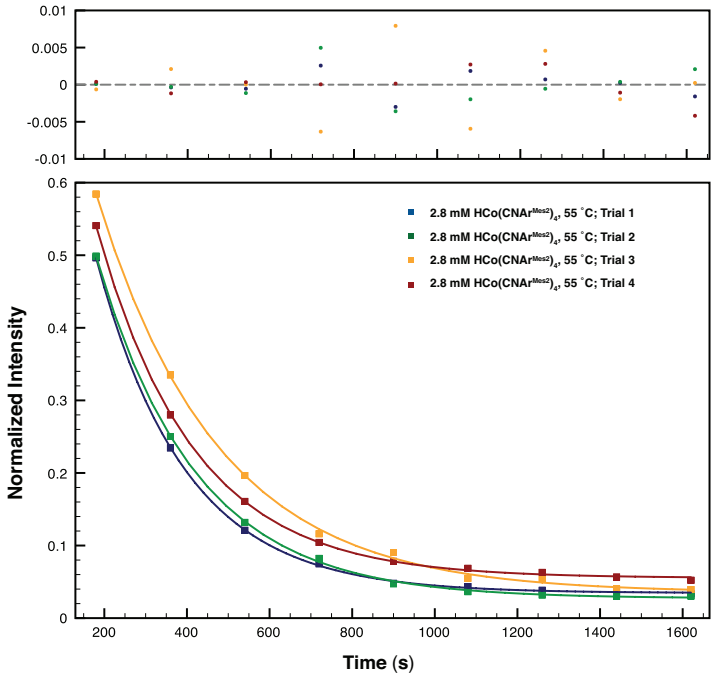

Figure S2.13. Decay of 2.8 mM $HCo(CNAr^{Mes2})_4$ (**1**) at 55 ˚C in C_6D_6. Bottom: Normalized intensity vs. time with non-linear least squares fit (4 trials). Top: Plot of residuals from the difference between observed experimental intensity and the predicted intensity obtained from non-linear least squares fitting.

Table S2.11. Measured k_{obs} for the decay of 2.8 mM solutions of $HCo(CNAr^{Mes2})_4$ (**1**) at 55 ˚C in C_6D_6. Rate estimates were determined from a non-linear least squares best fit of [**1**] vs. time.

Time Interval 180-1620 seconds	k_{obs} (s^{-1})	Error	R^2
2.8 mM 55 ˚C Trial 1	4.6×10^{-3}	5.0×10^{-5}	0.999
2.8 mM 55 ˚C Trial 2	4.2×10^{-3}	6.4×10^{-5}	0.999
2.8 mM 55 ˚C Trial 3	3.4×10^{-3}	8.6×10^{-5}	0.999
2.8 mM 55 ˚C Trial 4	4.3×10^{-3}	5.5×10^{-5}	0.999
	Average k_{obs} (s^{-1})	St. Dev (σ)	–
Average	4.1×10^{-3}	5.2×10^{-4}	–

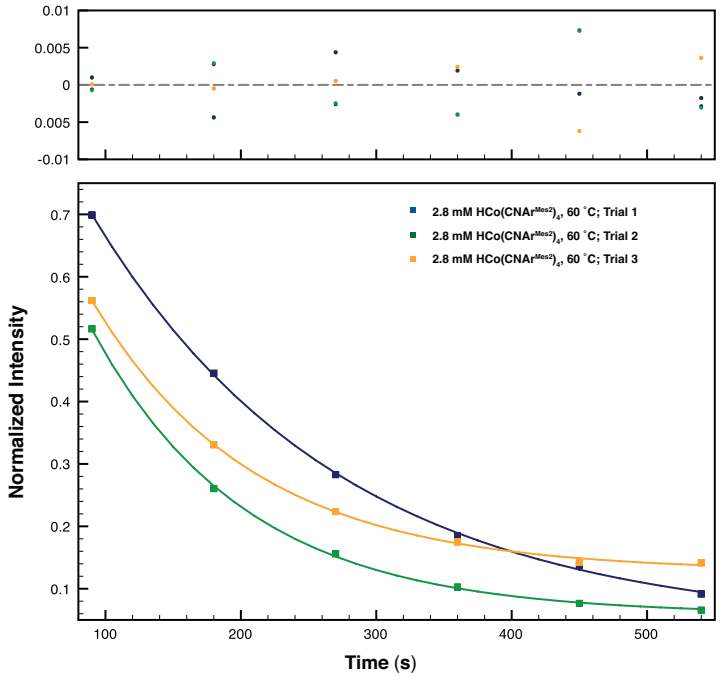

Figure S2.14. Decay of 2.8 mM $HCo(CNAr^{Mes2})_4$ (**1**) at 60 ˚C in C_6D_6. Bottom: Normalized intensity vs. time with non-linear least squares fit (3 trials). Top: Plot of residuals from the difference between observed experimental intensity and the predicted intensity obtained from non-linear least squares fitting.

Table S2.12. Measured k_{obs} for the decay of 2.8 mM solutions of $HCo(CNAr^{Mes2})_4$ (**1**) at 60 ˚C in C_6D_6. Rate estimates were determined from a non-linear least squares best fit of [**1**] vs. time.

Time Interval 90-540 seconds	k_{obs} (s^{-1})	Error	R^2
2.8 mM 60 ˚C Trial 1	5.5×10^{-3}	2.4×10^{-4}	0.999
2.8 mM 60 ˚C Trial 2	8.9×10^{-3}	2.6×10^{-4}	0.999
2.8 mM 60 ˚C Trial 3	8.4×10^{-3}	2.9×10^{-4}	0.999
	Average K_{obs} (s^{-1})	St. Dev (σ)	
Average	7.6×10^{-3}	1.8×10^{-3}	

Table S2.13. k_{obs} for the decay of 2.8 mM solutions of $HCo(CNAr^{Mes2})_4$ (**1**) over the temperature range 25-60 ˚C (5 ˚C increments) in C_6D_6.

2.8 mM $HCo(CNAr^{Mes2})_4$	k_{obs} (s^{-1})	St. Dev (σ)
25 ˚C (3 Trials)	$6.4x10^{-5}$	$2.5x10^{-6}$
30 ˚C (3 Trials)	$1.5x10^{-4}$	$6.1x10^{-6}$
35 ˚C (4 Trials)	$3.1x10^{-4}$	$4.0x10^{-4}$
40 ˚C (4 Trials)	$6.1x10^{-4}$	$5.8x10^{-5}$
45 ˚C (3 Trials)	$9.9x10^{-4}$	$1.4x10^{-4}$
50 ˚C (4 Trials)	$2.0x10^{-3}$	$8.0x10^{-5}$
55 ˚C (4 Trials)	$4.1x10^{-3}$	$5.2x10^{-4}$
60 ˚C (3 Trials)	$7.6x10^{-3}$	$1.8x10^{-3}$

S2.5. Eyring Analysis and Activation Parameters for the Decay of $HCo(CNAr^{Mes2})_4$ (2.8 mM, C_6D_6,)

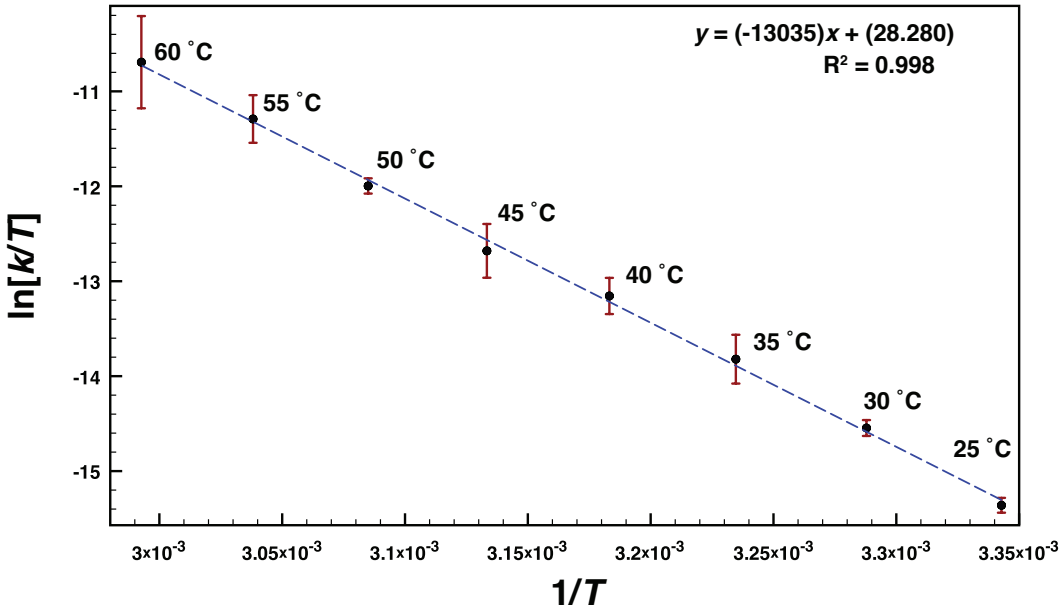

Figure S2.15. Eyring plot for the decay of $HCo(CNAr^{Mes2})_4$ (**1**) over the temperature range 25 – 60 ˚C (2.8 mM, C_6D_6; 5 ˚C increments). Error bars are derived from the standard deviation of each average k_{obs} value and plotted at ± 2σ (95 % confidence interval).

Table S2.14. Activation parameters for $HCo(CNAr^{Mes2})_4$ (**1**) decay in C_6D_6. Parameters were calculated using an Eyring analysis from averaged VT rate data plotted in Figure S2.15 and tabulated in Table S2.13.

Parameter	Calculated Value	Error (σ)
$\Delta H^{\ddagger}$ (kcal/mol)	26	1
$\Delta S^{\ddagger}$ (cal/mol*K)	9	2

S2.6 Estimation of k_{obs} for the Decay of $HCo(CNAr^{Mes2})_4$ (2.8mM, C_6D_6, 40 ˚C) in the presence of added $CNAr^{Mes2}$ (5 equiv, 14 mM).

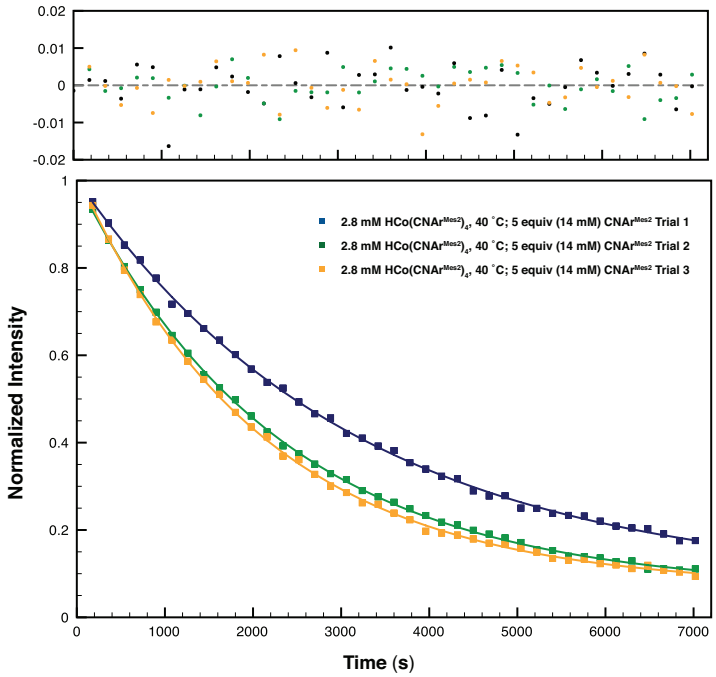

Figure S2.16. Decay of 2.8 mM $HCo(CNAr^{Mes2})_4$ (**1**) in the presence of $CNAr^{Mes2}$ (5.0 equiv, 14 mM) at 40 ˚C in C_6D_6. Bottom: Normalized intensity vs. time with non-linear least squares fit (3 trials). Top: Plot of residuals from the difference between observed experimental intensity and the predicted intensity obtained from non-linear least squares fitting.

Table S2.15. Estimated rate data for the decay of 2.8 mM C_6D_6 solutions of $HCo(CNAr^{Mes2})_4$ (**1**) in the presence of 5.0 equiv (14 mM) $CNAr^{Mes2}$ at 40 ˚C. Rate estimates were determined from a non-linear least squares best fit of [**1**] vs. time.

Time Interval 180-7020 seconds	k_{obs} (s^{-1})	Error	R^2
2.8 mM $HCo(CNAr^{Mes2})_4$ with 5 equiv (14 mM) $CNAr^{Mes2}$ at 40 ˚C Trial 1	$3.2x10^{-4}$	$5.3x10^{-6}$	0.999
2.8 mM $HCo(CNAr^{Mes2})_4$ with 5 equiv (14 mM) $CNAr^{Mes2}$ at 40 ˚C Trial 2	$4.4x10^{-4}$	$4.0x10^{-6}$	0.999
2.8 mM $HCo(CNAr^{Mes2})_4$ with 5 equiv (14 mM) $CNAr^{Mes2}$ at 40 ˚C Trial 3	$4.8x10^{-4}$	$5.0x10^{-6}$	0.999
	Average k_{obs} (s^{-1})	St. Dev (σ)	–
Average	$4.1x10^{-4}$	$8.4x10^{-5}$	–

Table S2.16. Average measured k_{obs} for the decay of 2.8 mM C_6D_6 solutions of $HCo(CNAr^{Mes2})_4$ (**1**) at 40 ˚C, compared to average measured k_{obs} for the decay of 2.8 mM C_6D_6 solutions of $HCo(CNAr^{Mes2})_4$ (**1**) in the presence of containing 5.0 equiv (14 mM) $CNAr^{Mes2}$ at 40 ˚C.

Time Interval 180-7020 seconds	k_{obs} (s^{-1})	St. Dev (σ)
$HCo(CNAr^{Mes2})_4$ 2.8 mM 40 ˚C (4 Trials)	$6.1x10^{-4}$	$5.8x10^{-5}$
$HCo(CNAr^{Mes2})_4$ 2.8 mM 40 ˚C with 5 equiv (14 mM) $CNAr^{Mes2}$ (3 Trials)	$4.1x10^{-4}$	$8.4x10^{-5}$

S3. Crystallographic Structure Determinations

General Methodology. Single-crystal X-ray structure determinations were carried out using Bruker Platform or Kappa X-ray diffractometers equipped with Mo or Cu radiation sources (sealed tube or rotating anode), low-temperature cryostats and CCD detectors (Bruker APEX or Bruker APEX II) at the UCSD Small-Molecule Crystallography Facility. All structures were solved by direct methods using SHElXS and refined by full-matrix least-squares procedures utilizing SHELXL within the Olex2 small-molecule solution, refinement and analysis software.[7,8] For cases of significant solvent disorder SQUEEZE was implemented.[8]

Structure Solution Details. The pentane molecule of co-crystallization in $HCo(CNAr^{Mes2})_4 \cdot 2(C_5H_{12})$ was disordered over two positions. This disorder was treated with a two-site positional disorder model and refined anisotropically. The hydride is disordered over four possible facial capping positions and was not unambiguously located. The cyclohexane molecule of co-crystallization in $HCo(CNAr^{Mes2})_4 \cdot 2(C_6H_{12})$ was disordered between two-possible chair conformations. This disorder was treated with a two-site positional disorder model and refined anisotropically. The hydride is disordered over four possible facial capping positions and was not located. The cobalt atom in $Co(\eta^6\text{-(Mes)-}\kappa^1\text{-}C\text{-C(H)NAr}^{Mes2})(CNAr^{Mes2})$ (**2**) is disordered over two positions along with the isocyanide and iminoacyl moieties. This disorder was modeled and refined anisotropically. Similar disorder was observed for $[Co(\eta^6\text{-(Mes)-}\kappa^1\text{-}C\text{-C(H)N(H)Ar}^{Mes2})(CNAr^{Mes2})]OTf$.

The solvent molecules of co-crystallization in $HCo(CNAr^{Mes2})_3(CN\textit{t}\text{-Bu}) \cdot 0.25(THF) \cdot 0.50(MeCN) \cdot 0.75(C_5H_{12})$ are compositionally disordered. The compositional disorder was fully modeled and refined anisotropically. The severely disordered Et_2O solvent molecule of co-crystallization in $HCo(CNAr^{Mes2})_3(CNXyl) \cdot Et_2O$ was treated with Squeeze. Squeeze found one void containing a single Et_2O molecule. Its formula was added to the formula for the unit cell and its electron density removed. The toluene solvent molecule of co-crystallization in $HCo(CNAr^{Mes2})_3(PPh_3) \cdot$toluene (**7**$^{\mathbf{PPh3}}$) was disordered end-over-end. This positional disorder was modeled and the atom positions anisotropically refined.

There is compositional disorder in the solvent molecules of co-crystallization for $Co(\kappa^1\text{-}C\text{-C[C(H)NAr}^{Mes2}]NAr^{Mes2})(CNAr^{Mes2})(CO)_3 \cdot 0.05(Toluene) \cdot 0.95(C_6H_{14})$. The major disorder component contains pentane at ~ 95 % occupancy and toluene at ~ 5 % occupancy. The disorder was modeled and refined.

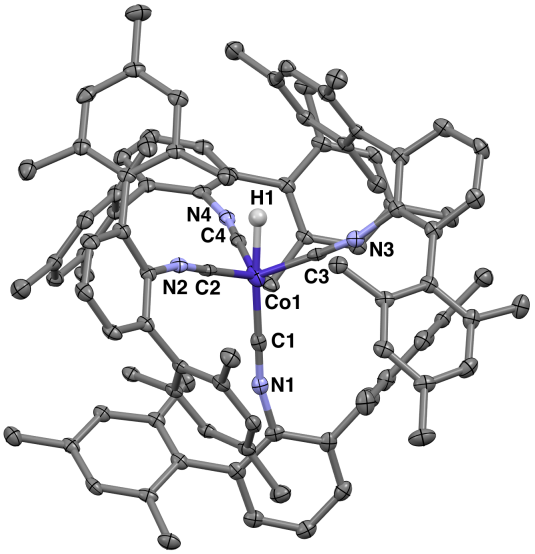

Figure S3.1. Molecular structure of $HCo(CNAr^{Mes2})_4 \cdot (C_5H_{12})$ (**1**$\cdot(C_5H_{12})$) in C2/c. Pentane solvent molecule omitted. One-component of the disordered hydride in its idealized position is shown. Selected bond distances (Å) and angles (˚). C1-Co1 =1.803 (3), C2-Co1 = 1.813(3), C3-Co1 = 1.813(3), C4-Co1 = 1.803(3), C1-Co1-C2 = 111.43 (10), C1-Co1-C3 =112.55(10), C1-Co1-C4 = 108.12(14), C2-Co1-C3 = 100.72 (13), C2-Co1-C4 = 112.55(10), C3-Co1-C4 = 111.43(10).

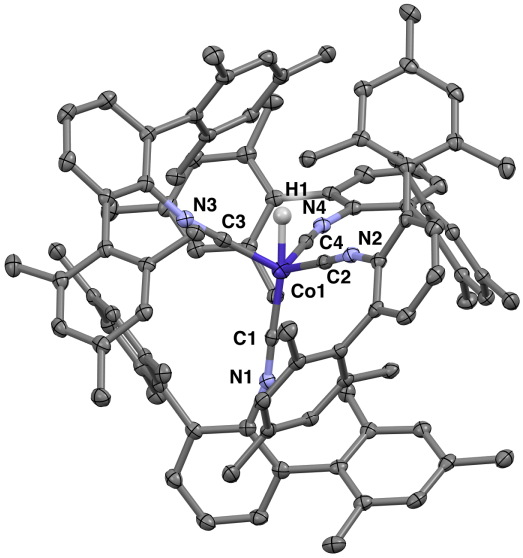

Figure S3.2. Molecular structure of $HCo(CNAr^{Mes2})_4 \cdot (C_6H_{12})$ (**1**$\cdot(C_6H_{12})$) in ($I\bar{4}\,2d$). Cyclohexane solvent molecule omitted. One-component of the disordered hydride in its idealized position is shown. Selected bond distances (Å) and angles (˚). C1-Co1 = 1.798(4), C2-Co1 = 1.798(4), C3-Co1 = 1.798(4), C4-Co1 = 1.798(4), C1-Co1-C2 = 112.51(12), C1-Co1-C3 =112.55(10), C1-Co1-C4 = 103.6(2), C2-Co1-C3 = 103.6(2), C2-Co1-C4 = 112.55(10), C3-Co1-C4 = 112.51(12).

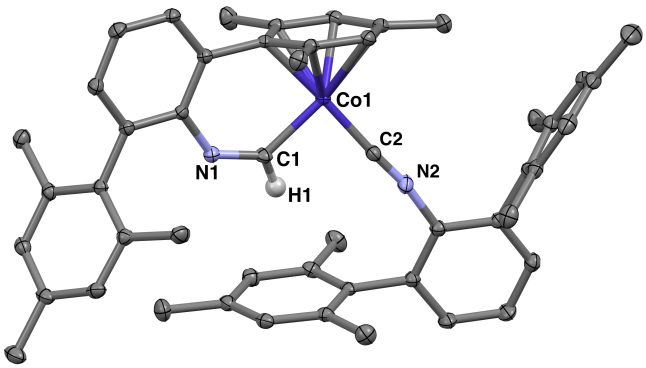

Figure S3.3. Molecular structure of Co(η^6-(Mes)-κ^1-C-C(H)NAr^{Mes2})(CNAr^{Mes2}) (**2**). One-component of the disordered cobalt atom is shown. Selected bond distances (Å) and angles (˚). Co1-C1 = 1.886(5), Co1-C2 = 1.788(7), C1-N1 = 1.271(7), Co1-C1-N1 = 129.4(4), Co1-C1-N2 = 175.4(5).

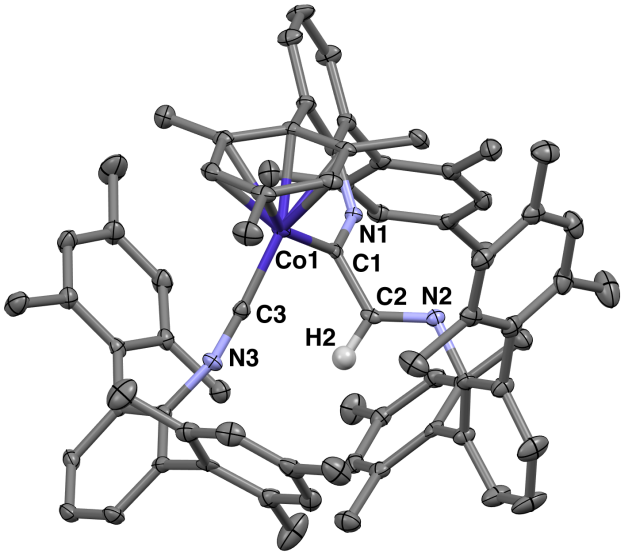

Figure S3.4. Molecular structure of Co(η^6-(Mes)-κ^1-C-C[C(H)NAr^{Mes2}]NAr^{Mes2})(CNAr^{Mes2}) (**3**). Selected bond distances (Å) and angles (˚). N1-C1 = 1.292(2), C1-C2 = 1.485(4), C2-N2 = 1.270(3), C1-Co1 = 1.911(2), C3-Co1 = 1.779(2), N1-C1-C2 = 115.7(2), C1-C2-N2 = 121.5(2).

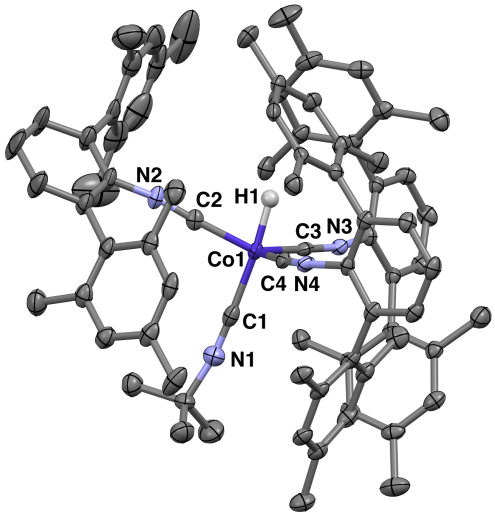

Figure S3.5. Molecular structure of $HCo(CNAr^{Mes2})_3(CNt\text{-}Bu)\cdot 0.25(THF)\cdot 0.50(MeCN)\cdot 0.75(C_5H_{12})$, ($\mathbf{4}^{\mathbf{tBuNC}}\cdot 0.25(THF)\cdot 0.50(MeCN)\cdot 0.75(C_5H_{12})$). Two unique molecules crystallized in the assymetric unit. One is omitted. Compositionally disordered solvent molecules are also omitted. Selected bond distances (Å) and angles (˚). C1-Co1 = 1.850(4), C2-Co1 = 1.802(3), C3-Co1 = 1.802(4), C4-Co1 = 1.806(3), H1-Co1 = 1.43(3), C1-Co1-H1 = 173(1), C1-Co1-C2 = 95.9(1), C1-Co1-C3 = 99.3(1), C1-Co1-C4 = 99.7(1), C2-Co1-C3 = 127.3(1), C2-Co1-C4 = 117.2(1), C3-Co1-C4 = 109.4(1).

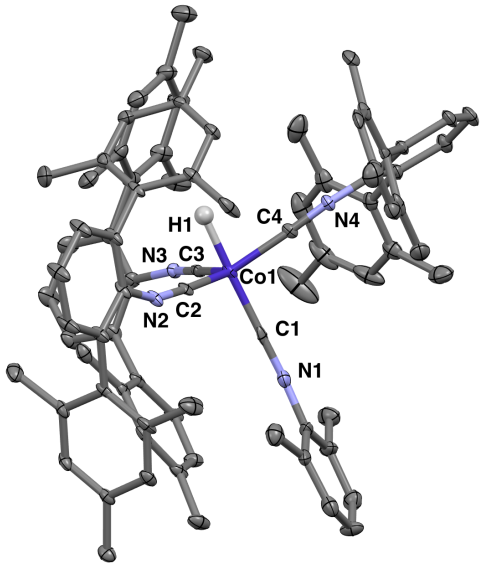

Figure S3.6. Molecular structure of $HCo(CNAr^{Mes2})_3(XylylNC)\cdot(Et_2O)$ ($\mathbf{4}^{\mathbf{XylylNC}}\cdot Et_2O$). Solvent molecule of co-crystalization omitted. Selected bond distances (Å) and angles (˚). C1-Co1 = 1.790(5), C2-Co1 = 1.804(4), C3-Co1 = 1.812(5), C4-Co1 = 1.803(3), Co1-H1 = 1.54(5), C1-Co1-H1 = 176(2), C1-Co1-C2 = 99.4(2), C1-Co1-C3 = 94.2(2), C1-Co1-C4 = 98.6(2), C2-Co1-C3 = 115.6(2), C2-Co1-C4 = 120.0(2), C3-Co1-C4 = 119.5(2).

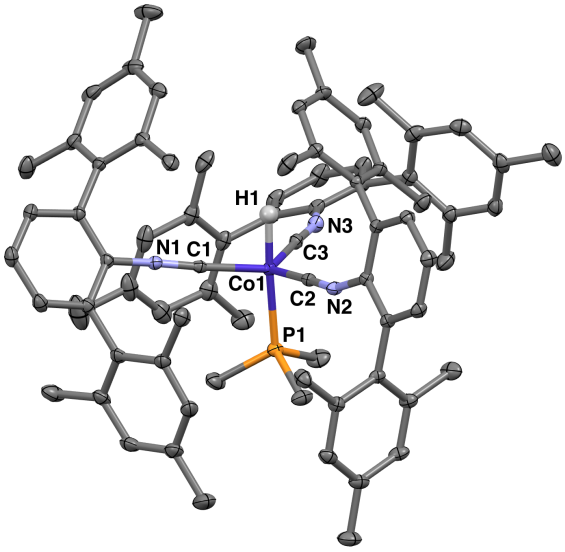

Figure S3.7. Molecular structure of $HCo(CNAr^{Mes2})_3(PMe_3)\cdot(MeCN)$ ($\mathbf{4}^{\mathbf{PMe3}}\cdot(MeCN)$). Solvent molecule of co-crystalization omitted. Selected bond distances (Å) and angles (˚). P1-Co1 = 2.1793(5), C1-Co1 = 1.790(2), C2-Co1 = 1.806(1), C3-Co1 = 1.792(1), H1-Co1 = 1.46(2), P1-Co1-C1 = 94.78(5), P1-Co1-C2 = 98.88(5), P1-Co1-C3 = 93.64(5), C1-Co1-C2 = 114.73(6), C2-Co1-C3 = 120.47(6), c1-Co1-C3 = 121.85(6).

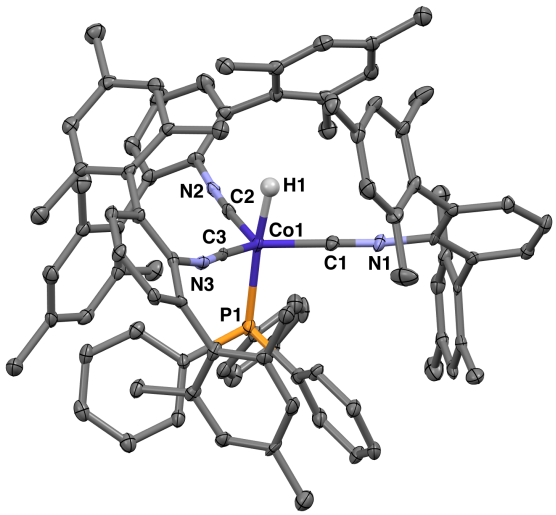

Figure S3.8. Molecular structure of $HCo(CNAr^{Mes2})_3(PPh_3)\cdot(C_7H_8)$ ($\mathbf{4}^{\mathbf{PPh3}}\cdot(C_7H_8)$). Solvent molecule of co-crystalization omitted. Selected bond distances (Å) and angles (˚). P1-Co1 = 2.184(2), Co1-C1 = 1.802(6), Co1-C2 = 1.821(7), Co1-C3 = 1.800(6), Co1-H1 = 1.58(6), P1-Co1-C1 = 97.1(2), P1-Co1-C2 = 97.0(2), P1-Co1-C3 = 95.2(2), C1-Co1-C2 = 117.5(3), C1-Co1-C3 = 125.1(3), C2-Co1-C3 = 113.7(3), p1-Co1-H = 173(2).

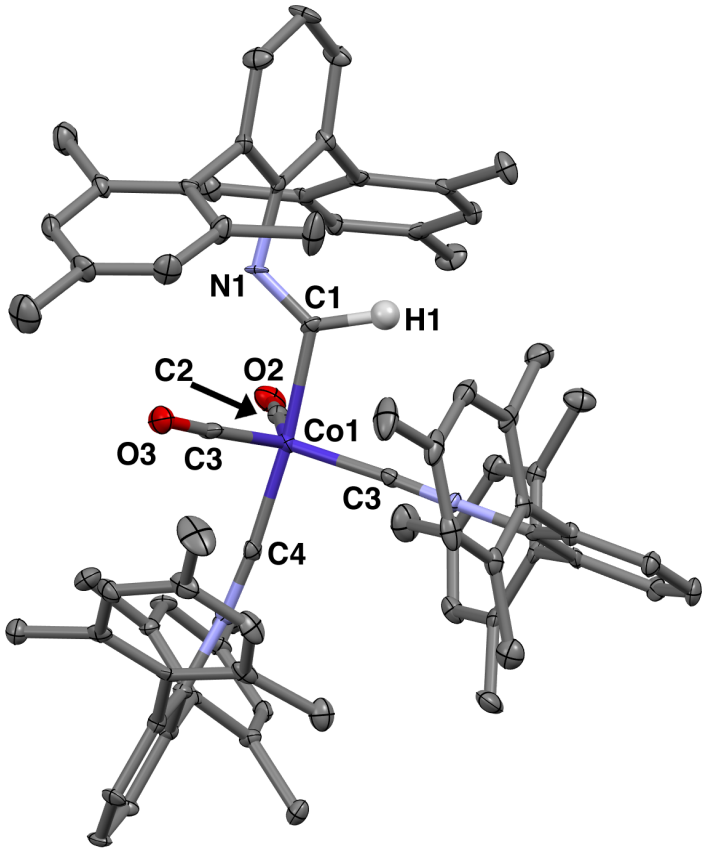

Figure S3.9. Molecular structure of $Co(\kappa^1\text{-}C\text{-}C(H)=NAr^{Mes2})(CNAr^{Mes2})_2(CO)_2\cdot(C_6H_{14})$ (**5**·(C_6H_{14})). Hexane solvent molecule of co-crystallization omitted. Selected bond distances (Å) and angles (˚). Co1-C1 = 1.959(5), Co1-C2 = 1.764(8), Co1-C3 = 1.789(8), Co1-C4 = 1.855(5), Co1-C5 = 1.848(5), C1-N1 = 1.264(7), C1-H1 = 0.948, N1-C1-Co1 = 124.3(4), C1-Co1-C2 = 86.6(3), C1-Co1-C3 = 84.4(3), C1-Co1-C4 = 92.9(2).

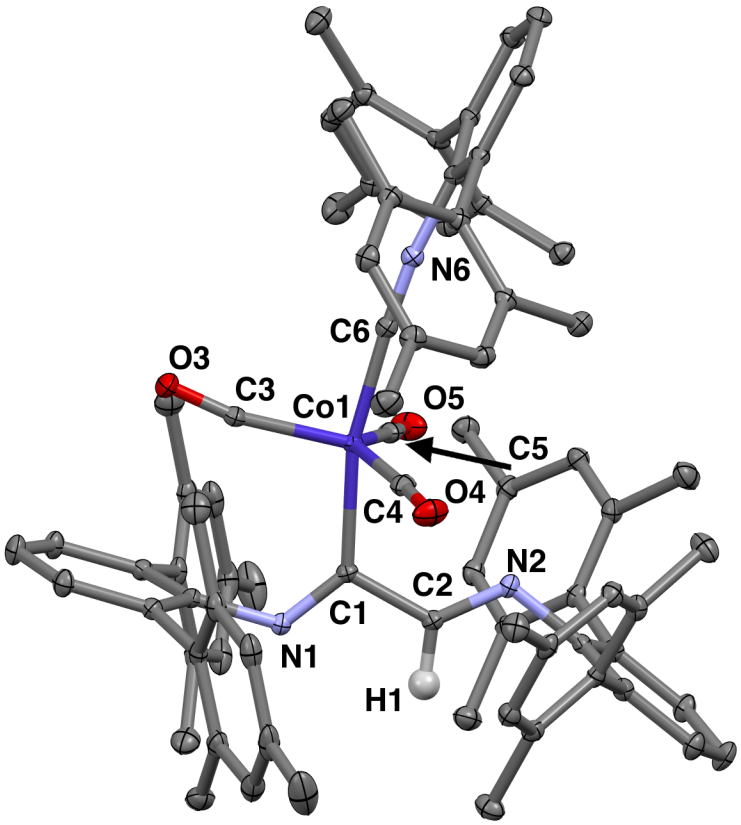

Figure S3.10. Molecular structure of Co(κ^1-C-^{Mes2}ArNC(H)CNAr^{Mes2})(CNAr^{Mes2})(CO)$_3$·0.05(C_7H_8)·0.95(C_6H_{14}) (**6**·0.05(C_7H_8)·0.95(C_6H_{14})). Compositionally disordered toluene/pentane molecules of co-crystalization are omitted. Selected bond distances (Å) and angles (˚). N1-C1 = 1.270(3), C1-C2 = 1.499(3), C2-N2 = 1.265(3), C1-Co1 = 2.004(2), N1-C1-C2 = 111.4(2), C1-C2-N2 = 125.3(2).

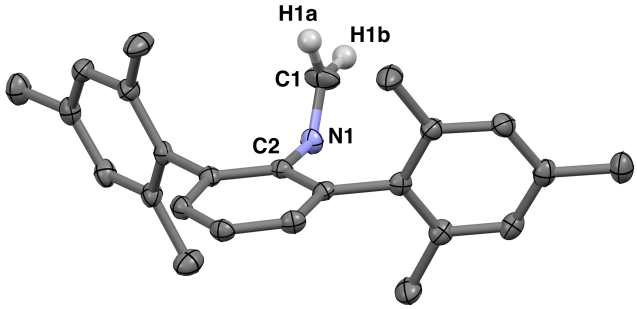

Figure S3.11. Molecular structure of 1,1-H_2C=NAr^{Mes2} (**7**). Selected bond distances (Å) and angles (˚). C1-N1 = 1.247(5), 1.429(4), C1-N1-C2 = 120.0(3).

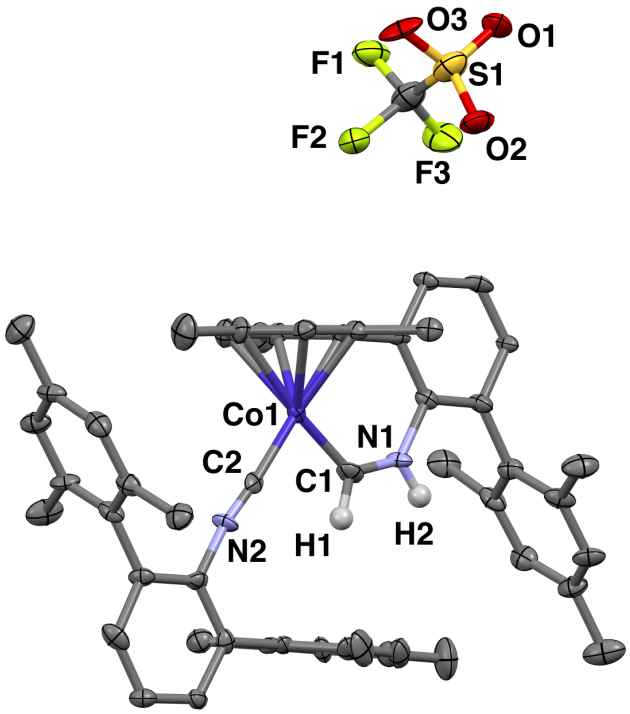

Figure S3.12. Molecular structure of [Co(η^6-(Mes)-κ^1-C-C(H)N(H)Ar^{Mes2})($CNAr^{Mes2}$)]OTf ($\mathbf{7}^{OTf}$). Selected bond distances (Å) and angles (˚). Co1-C1 = 1.82(2), C1-N1 = 1.34(2), Co1-C2 = 1.83(2), N1-C1-Co1 = 127(1), C1-Co1-C2 = 88.7(7).

Table S3.1. Crystallographic data collection and refinement information.

	$HCo(CNAr^{Mes2})_4 \cdot 2(C_5H_{12})$ (**1**·$2(C_5H_{12})$)	$HCo(CNAr^{Mes2})_4 \cdot 2(C_6H_{12})$ (**1**·$2(C_6H_{12})$)	$Co(\eta^6\text{-(Mes)-}\kappa^1\text{-}C\text{-}C(H)NAr^{Mes2})(CNAr^{Mes2})$ (**2**)
Formula	$C_{110}H_{125}CoN_4$	$C_{110}H_{128}CoN_4$	$C_{50}H_{51}CoN_2$
Crystal System	Monoclinic	Tetragonal	Triclinic
Space Group	*C*2/*c*	$I\bar{4}\,2d$	$P\bar{1}$
a, Å	29.856(3)	27.4917(8)	11.3496(5)
b, Å	11.6893(11)	27.4917(8)	15.7745(7)
c, Å	27.498(3)	11.7280(5)	18.5671(8)
α, deg	90	90	94.906(3)
β, deg	111.766(2)	90	106.630(3)
γ, deg	90	90	110.407(2)
V, Å^3	8912.7(14)	8863.9(6)	2921.0(2)
Z	4	4	4
Radiation (λ, Å)	Mo-Kα, 0.71073	Cu-Kα, 1.54184	Mo-Kα, 0.71073
ρ (calcd.), g/cm^3	1.164	1.191	1.261
μ, mm^{-1}	0.244	1.906	0.478
Temp, K	100(2)	100(2)	90(2)
θ max, deg	26.443	58.656	30.822
data/restraints/ parameters	9141 / 12 / 585	3122 / 16 / 284	17921 / 0 / 780
R_1	0.0564	0.0369	0.0548
wR_2	0.1455	0.0923	0.1236
GOF	1.022	1.042	1.033

Table S3.2. Crystallographic data collection and refinement information.

	Co(η^6-(Mes)-κ^1-*C*-C[C(H)NAr^{Mes2}]NAr^{Mes2})(CNAr^{Mes2}) (**3**)	1,1-H_2C=NAr^{Mes2} (**7**)	[Co(η^6-(Mes)-κ^1-*C*-C(H)N(H)Ar^{Mes2})(CNAr^{Mes2})]OTf
Formula	$C75H_{76}CoN_3$	$C_{25}H_{27}N$	$C_{51}H_{52}CoF_3N_2O_3S$
Crystal System	Triclinic	Orthorhombic	Orthorhombic
Space Group	$P\bar{1}$	*Pnma*	$Pca2_1$
a, Å	11.0857(3)	6.4717(7)	14.8625(14)
b, Å	12.2740(4)	23.848(2)	12.9587(11)
c, Å	24.3169(8)	12.7063(13)	23.5511(18)
α, deg	104.3050(10)	90	90
β, deg	94.5650(10)	90	90
γ, deg	105.8240(10)	90	90
V, Å^3	3046.04(16)	1961.0(3)	4356.2(7)
Z	2	4	4
Radiation (λ, Å)	Mo-Kα, 0.71073	Cu-Kα, 1.54184	Mo-Kα, 0.71073
ρ (calcd.), g/cm^3	1.176	1.157	1.138
μ, mm^{-1}	0.327	0.497	0.291
Temp, K	100(2)	100(2)	100(2)
θ max, deg	24.38	65.193	25.382
data/restraints/parameters	10303 / 0 / 734	1586 / 0 / 133	6617 / 26 / 585
R_1	0.0434	0.0564	0.0719
wR_2	0.0939	0.1306	0.1538
GOF	1.019	1.057	1.013

Table S3.3. Crystallographic data collection and refinement information.

	$HCo(CNAr^{Mes2})_3$ (CN*t*-Bu)·0.25(THF)· 0.50(MeCN)· 0.75(C_5H_{12}) (**4**^{CNtBu})·0.25(THF)· 0.50(MeCN)· 0.75(C_5H_{12})	$HCo(CNAr^{Mes2})_3$ (CNXyl)·(Et_2O) (**4**^{CNXyl}·(Et_2O))	$HCo(CNAr^{Mes2})_3$ (PMe_3)·(MeCN) (**4**^{PMe3}·(MeCN))
Formula	$C_{171.25}H_{186.75}Co_2N_{8.5}O_{0.25}$	$C_{90}H_{100}CoN_4O_1$	$C_{80}H_{88}CoN_4P$
Crystal System	Triclinic	Tetragonal	Triclinic
Space Group	$P\bar{1}$	$P\bar{1}$	$P\bar{1}$
a, Å	14.7093(6)	13.365(4)	13.363(2)
b, Å	20.7346(8)	14.291(4)	15.442(2)
c, Å	24.4313(11)	21.974(5)	17.940(3)
α, deg	88.505(2)	104.196(8)	98.851(5)
β, deg	84.345(2)	90.338(9)	91.101(5)
γ, deg	86.6950	116.827(8)	110.393(4)
V, Å^3	7401.2(5)	3597.8(16)	3417.8(9)
Z	2	2	2
Radiation (λ, Å)	Mo-Kα, 0.71073	Mo-Kα, 0.71073	Mo-Kα, 0.71073
ρ (calcd.), g/cm^3	1.115	1.151	1.162
μ, mm^{-1}	0.278	0.286	0.320
Temp, K	100(2)	90(2)	100(2)
θ max, deg	25.439	25.563	30.210
data/restraints/ parameters	27144 / 31 / 1710	9900 / 4 / 825	19102 / 9 /810
R_1	0.0631	0.0612	0.0376
wR_2	0.1545	0.01338	0.0953
GOF	1.036	1.016	1.016

Table S3.4. Crystallographic data collection and refinement information.

	$HCo(CNAr^{Mes2})_3(PPh_3)\cdot(C_7H_8)$ ($\mathbf{4}^{PPh3}\cdot(C_7H_8)$)	$Co(\kappa^1\text{-}C\text{-}C(H)NAr^{Mes2})(CNAr^{Mes2})(CO)_2\cdot(C_6H_{14})$ ($\mathbf{5}\cdot(C_6H_{14})$)	$Co(\kappa^1\text{-}C\text{-}C[C(H)NAr^{Mes2}]NAr^{Mes2})(CO)_3\cdot 0.05(C_7H_8)\cdot 0.95(C_6H_{14})$ ($\mathbf{6}\cdot 0.05(C_7H_8)\cdot 0.95(C_6H_{14})$)
Formula	$C_{100}H_{99}CoN_3P$	$C_{82}H_{88}CoN_3O_2$	$C_{80}H_{88}CoN_4P$
Crystal System	Monoclinic	Monoclinic	Orthorhombic
Space Group	*C*2/*c*	$P2_1/c$	*Pnma*
a, Å	22.971(9)	19.424(2)	26.2209(13)
b, Å	15.184(5)	14.2969(12)	18.8401(9)
c, Å	43.841(5)	26.503(2)	14.1228(7)
α, deg	90	90	90
β, deg	94.636(19)	106.846(4)	90
γ, deg	90	90	90
V, Å^3	15242(9)	7044.1(11)	6976.7(6)
Z	8	4	4
Radiation (λ, Å)	Mo-Kα, 0.71073	Mo-Kα, 0.71073	Mo-Kα, 0.71073
ρ (calcd.), g/cm^3	1.209	1.138	1.179
μ, mm^{-1}	0.296	0.291	0.297
Temp, K	100(2)	100(2)	100(2)
θ max, deg	23.547	22.030	25.481
data/restraints/ parameters	9522 / 0 / 942	8617 / 48 / 829	6678 / 28 / 455
R_1	0.0716	0.0646	0.0392
wR_2	0.1253	0.1205	0.1049
GOF	0.978	0.986	1.028

S4. References

(1) Pangborn, A. B.; Giardello, M. A.; Grubbs, R. H.; Rosen, R. K.; Timmers, F. J. *Organometallics* **1996**, *15*, 1518–1520.

(2) Arnarego, W. L.; Chai, C. L. *Purification of Laboratory Chemicals*; 5 ed.; Elsevier: Oxford, 2003.

(3) Fox, B. J.; Sun, Q. Y.; Dipasquale, A. G.; Fox, A. R.; Rheingold, A. L.; Figueroa, J. S. *Inorg. Chem.* **2008**, *47*, 9010–9020.

(4) Carpenter, A. E.; Margulieux, G. W.; Millard, M. D.; Moore, C. E.; Weidemann, N.; Rheingold, A. L.; Figueroa, J. S. *Angew. Chem. Int. Ed.* **2012**, *51*, 9412–9416.

(5) Margulieux, G. W.; Weidemann, N.; Lacy, D. C.; Moore, C. E.; Rheingold, A. L.; Figueroa, J. S. *J. Am. Chem. So.c* **2010**, *132*, 5033–5035.

(6) Bruno, I. J.; Cole, J. C.; Edgington, P. R.; Kessler, M.; Macrae, C. F.; McCabe, P.; Pearson, J.; Taylor, R. *Acta Crystallogr B Struct. Sci.* **2002**, *58*, 389–397.

(7) Sheldrick, G. M. *Acta Crystallogr A Found Crystallogr.* **2008**, *64*, 112–122.

(8) Dolomanov, O. V.; Bourhis, L. J.; Gildea, R. J.; Howard, J. A. K.; Puschmann, H. *J. Appl. Crystallogr.* **2009**, *42*, 339–341.

(9) van der Sluis, P.; Spek, A. L. *Acta Crystallogr A Found Crystallogr.* **1990**, *46*, 194–201.